

Rough volatility: fact or artefact?

Rama Cont and Purba Das*
Mathematical Institute, University of Oxford

March 29, 2022

Abstract

We investigate the statistical evidence for the use of ‘rough’ fractional processes with Hurst exponent $H < 0.5$ for the modeling of volatility of financial assets, using a model-free approach. We introduce a non-parametric method for estimating the roughness of a function based on discrete sample, using the concept of normalized p -th variation along a sequence of partitions. We investigate the finite sample performance of our estimator for measuring the roughness of sample paths of stochastic processes using detailed numerical experiments based on sample paths of fractional Brownian motion and other fractional processes. We then apply this method to estimate the roughness of realized volatility signals based on high-frequency observations. Detailed numerical experiments based on stochastic volatility models show that, even when the instantaneous volatility has diffusive dynamics with the same roughness as Brownian motion, the realized volatility exhibits rough behaviour corresponding to a Hurst exponent significantly smaller than 0.5. Comparison of roughness estimates for realized and instantaneous volatility in fractional volatility models with different values of Hurst exponent shows that, irrespective of the roughness of the spot volatility process, realized volatility always exhibits ‘rough’ behaviour with an apparent Hurst index $\hat{H} < 0.5$. These results suggest that the origin of the roughness observed in realized volatility time-series lies in the microstructure noise rather than the volatility process itself.

*Purba.Das@maths.ox.ac.uk

Contents

1	Introduction	3
1.1	Fractional processes in finance: from long-range dependence to ‘rough volatility’	3
1.2	Contribution	4
2	Measuring the roughness of a path	4
2.1	p -th variation and roughness index of a path	4
2.2	Normalized p -th variation	6
2.3	Estimating roughness from discrete observations	8
2.4	Finite sample behaviour of the roughness estimator	8
3	Spot volatility and realized volatility	13
4	Simulation experiments	15
4.1	Stochastic volatility diffusion models	15
4.2	A fractional Ornstein-Uhlenbeck model	22
5	Application to high-frequency financial data	25
5.1	AAPL	25
5.2	SP500	25
6	Rough volatility ... or microstructure noise?	27

1 Introduction

1.1 Fractional processes in finance: from long-range dependence to ‘rough volatility’

Beginning with Mandelbrot and VanNess [22], fractional Brownian motion and fractional Gaussian noise have been used as building blocks of stochastic models of various phenomena in physics, engineering [21] and finance [2, 5, 7, 9, 16, 26, 28]. Fractional Brownian motion has two remarkable properties which have contributed towards its adoption as a building block in stochastic models: first, its ability to model long-range dependence, as measured by the slow decay $\sim T^{2H-2}$ of auto-correlation functions of increments, where $0 < H < 1$ is the Hurst exponent; second, its ability to generate trajectories which have varying levels of Hölder regularity (‘roughness’). The former is a property that manifests itself over long time scales while the latter manifests itself over short time scales and, in general, these two properties are unrelated. But in the case of fractional Brownian motion, the two properties are linked through self-similarity and governed by the Hurst exponent $0 < H < 1$: for $H > 1/2$ one obtains long-range dependence in increments and trajectories smoother than Brownian motion while for $H < 1/2$ one obtains ‘anti-correlated’ increments and trajectories rougher than Brownian motion¹. Processes driven by fractional Gaussian noise with $H < 1/2$ are thus sometimes referred to as ‘rough processes’.

In early applications to financial data [2, 5, 7, 28], fractional processes were adopted in order to model *long range dependence* effects in financial time series [8]. More specifically, statistical evidence of *volatility clustering* [9] - positive dependence of the amplitude of returns over long time scales - led to the development of stochastic volatility models driven by fractional Brownian motion. A well-known example of such a fractional stochastic volatility model is the one proposed by Comte and Renault [7] who modelled the dynamics of the (instantaneous) volatility $\sigma(t)$ of an asset as:

$$Y(t) = \ln \sigma(t) \quad dY(t) = -\gamma Y(t)dt + \theta dB^H(t) \quad (1)$$

where B^H is a fractional Brownian motion (fBM) with Hurst exponent H . This long-range dependence in volatility is modelled by choosing $1 > H > 1/2$ [7, 5, 6, 18, 20].

A recent strand of literature, starting with Gatheral et al. [16], has suggested the use of fractional Brownian models with $H < 1/2$ for modelling volatility. The motivation of this approach, beginning with [16], is that empirical data on volatility estimators suggest that volatility is ‘rough’ i.e., has a (Hölder) roughness which is strictly less than 1/2. Unlike previous studies based on auto-correlations of various volatility estimators over long time scales [2, 5, 8], rough volatility models [16] rely on the analysis of the behaviour of volatility estimators over very short intraday time scales in order to assess the ‘roughness’ of these signals.

However, it has not been lost on experts working in this area that the estimation results in the previous literature on long-range dependence in volatility, which pointed out towards Hurst exponents $H > 0.5$ (and around 0.55) [2, 7, 20] seem to contradict the claims in the recent ‘rough volatility’ literature, which points to values of H much smaller than 0.5 (closer to 0.1). Together with the well-known statistical issues plaguing the estimation of Hurst exponents [4, 25], these conflicting results call for a critical examination of the empirical evidence for ‘rough volatility’.

Compounding this issue is the fact that (spot) volatility is not directly observed but estimated from data with an inherent estimation error, known in the context of high-frequency data as ‘microstructure noise’, which has been the subject of many studies [3, 19, 20]. This

¹Incidentally, Hurst and Hölder happen to have the same initials, adding to the confusion...

microstructure noise is far from IID: it is known to possess path-dependent features [19]. As a result, measures of roughness for realized volatility indicators may be quite different from those of the underlying ‘spot volatility’. This is simply because the convergence of high-frequency volatility estimators in L^p norms does not imply in any way their functional convergence in Hölder norms or other norms related to roughness.

1.2 Contribution

In the paper, we address these questions in detail by re-examining the statistical evidence from high-frequency financial data, in an attempt to clarify whether the assertion that ‘volatility is rough’ (i.e. rougher than typical paths of Brownian motion) is supported by empirical evidence. We investigate the statistical evidence for the use of ‘rough’ fractional processes with Hurst exponent $H < 0.5$ for the modelling of volatility of financial assets, using a non-parametric, model-free approach.

We introduce a non-parametric method for estimating the roughness of a function/path based on a (high-frequency) discrete sample, using the concept of normalized p -th variation along a sequence of partitions, and discuss the consistency of our estimator in a pathwise setting. We investigate the finite sample performance of our estimator for measuring the roughness of sample paths of stochastic processes using detailed numerical experiments based on sample paths of fractional Brownian motion and other fractional processes. We then apply this method to estimate the roughness of realized volatility signals based on high-frequency observations. Through a detailed numerical experiment based on a stochastic volatility model, we show that even when the instantaneous (spot) volatility has diffusive dynamics with the same roughness as Brownian motion, the realized volatility exhibits rough behaviour corresponding to a Hurst exponent significantly smaller than 0.5. Similar behavior is observed in financial data as well, which suggests that the origin of the roughness observed in realized volatility time-series lie in the estimation error rather than the volatility process itself. Comparison of roughness estimates for realized and instantaneous volatility in fractional volatility models for different values of Hurst parameter H shows that whatever the value of H for the (spot) volatility process, realized volatility always exhibits ‘rough’ behaviour.

Our results are broadly consistent with the points raised by Rogers [25], but we pinpoint more precisely the origin of the apparent ‘rough’ behaviour of volatility as being the microstructure noise inherent in the estimation of realized volatility. In particular, our results question whether the empirical evidence presented from high-frequency volatility estimates supports the ‘rough volatility’ hypothesis.

2 Measuring the roughness of a path

Determining the roughness of realized volatility from a sample path plays a crucial role in model specification [16, 14]. In practice, we observe only a single price path so one is faced with the problem of determining the roughness of a process from a single price path sampled at high frequency. We present in this section several concepts for measuring the roughness of a path, and discuss how they may be used to design estimators from high frequency observations.

2.1 p -th variation and roughness index of a path

Consider a sequence of partitions $\pi = (\pi^n)_{n \geq 1}$ of $[0, T]$ where

$$\pi^n = \left(0 = t_0^n < t_1^n < \cdots < t_{N(\pi^n)}^n = T\right) \quad (2)$$

represents observation times 'at frequency n '. We denote $N(\pi^n)$ to be the number of intervals in the partition π^n . Denote respectively by $|\pi^n| = \sup_{i=1, \dots, N(\pi^n)} |t_i^n - t_{i-1}^n|$, and $\underline{\pi}^n = \inf_{i=1, \dots, N(\pi^n)} |t_i^n - t_{i-1}^n|$, the size of the largest and the smallest interval of π^n . In this paper we will always assume

$$|\pi^n| = \sup_{i=1, \dots, N(\pi^n)} |t_i^n - t_{i-1}^n| \xrightarrow{n \rightarrow \infty} 0.$$

The concept of p -th variation along a sequence of partitions $\pi = (\pi^n)_{n \geq 1}$ with $0 = t_0^n < \dots < t_k^n < \dots < t_{N(\pi^n)}^n = T$ is defined following [12]:

Definition 1. (*p -th variation along a sequence of partitions*) $x \in C^0([0, T], \mathbb{R})$ has finite p -th variation along the sequence of partitions $\pi = (\pi^n, n \geq 1)$ if there exists a continuous increasing function $[x]_\pi^{(p)} : [0, T] \rightarrow \mathbb{R}_+$ such that

$$\forall t \in [0, T], \quad \sum_{\substack{[t_j^n, t_{j+1}^n] \in \pi^n: \\ t_j^n \leq t}} |x(t_{j+1}^n) - x(t_j^n)|^p \xrightarrow{n \rightarrow \infty} [x]_\pi^{(p)}(t). \quad (3)$$

If this property holds, then the convergence in (3) is uniform. We call $[x]_\pi^{(p)}$ the p -th variation of x along the sequence of partitions π . We denote $V_\pi^p([0, T], \mathbb{R})$ the set of all continuous paths with finite p -th variation along π .

Remark 1. For $x \in V_\pi^p([0, T], \mathbb{R})$ we have $[x]_\pi^{(p)}(T) < \infty$. If

$$\sum_{\pi^n \cap (a, b)} |x(t_{i+1}^n) - x(t_i^n)|^p \rightarrow \infty$$

for all $(a, b) \subset [0, T]$ then we will write $[x]^{(p)}(t) = \infty$.

To formalize the concept of roughness, we introduce the notion of variation index and roughness index of a path:

Definition 2 (Variation index). The variation index of a path x along a partition sequence π is defined as the smallest $p \geq 1$ for which x has finite p -th variation along π :

$$p^\pi(x) = \inf \{p \geq 1 : x \in V_\pi^p([0, T], \mathbb{R})\}.$$

Definition 3 (Roughness index). The roughness index of a path x (along π) is defined as

$$H^\pi(x) = \frac{1}{p^\pi(x)}.$$

When the underlying sequence of partitions is clear, we will omit π and denote these indices as $p(x)$ and $H(x)$.

For a (real-valued) stochastic process $X : [0, T] \times \Omega \rightarrow \mathbb{R}$ the roughness index $p^\pi(X(., \omega))$ of each sample path $X(., \omega)$ may be different in principle. Nevertheless there are many important classes of stochastic processes which have an *almost-sure* roughness index. For example, the roughness index of fractional Brownian motion (fBM) matches with the corresponding Hurst parameter/ Hölder exponent:

Example 1. Brownian motion B has variation index $p^\pi(B) = 2$ and roughness index $H^\pi(B) = \frac{1}{2}$ along any refining partition sequence π or any partition π with $|\pi^n| \log n \rightarrow 0$ [13].

Fractional Brownian motion B^H has variation index $p^\mathbb{T}(B^H) = \frac{1}{H}$ and roughness index $H^\mathbb{T} = H$ along the dyadic partition sequence \mathbb{T} .

In general, the existence of a variation index is not obvious. Along the lines of [17, Proposition 2.3] we give a necessary and sufficient condition for the existence of variation index. Define, $q^+(x, \pi)$ and $q^-(x, \pi)$ as follows:

$$q^+(x, \pi) := \sup_{p>0} \left\{ \limsup_{n \uparrow \infty} \sum_{\pi^n} |x(t_{i+1}^n) - x(t_i^n)|^p = \infty \right\} \text{ and,}$$

$$q^-(x, \pi) := \sup_{p>0} \left\{ \liminf_{n \uparrow \infty} \sum_{\pi^n} |x(t_{i+1}^n) - x(t_i^n)|^p = \infty \right\}.$$

Lemma 2.1 (Existence of variation index). *Let $x \in C^0([0, T], \mathbb{R})$. For any partition sequence π with vanishing mesh, the variation index $p^\pi(x)$ exists if and only if $q^+(x, \pi) = q^-(x, \pi)$. In this case, $p^\pi(x) = q^+(x, \pi) = q^-(x, \pi)$.*

The following lemma [10] shows how the variation index establishes a 'roughness scale' in terms of the p -th variation:

Lemma 2.2. *Let π be a sequence of partitions with vanishing mesh $|\pi^n| \downarrow 0$. If $x \in C^0([0, T], \mathbb{R})$ has variation index $p^\pi(x)$ and $x \in V_\pi^{p^\pi(x)}([0, T], \mathbb{R})$ then:*

$$[x]_\pi^{(q)}(t) = \begin{cases} 0 & \text{if } q > p^\pi(x) \\ 0 \leq [x]_\pi^{(p)} < \infty & \text{if } q = p^\pi(x) \\ \infty & \text{if } q < p^\pi(x) \end{cases} \quad (4)$$

$x \in C^0([0, T], \mathbb{R})$ is said to be rougher than $y \in C^0([0, T], \mathbb{R})$ along π if $p^\pi(y) < p^\pi(x)$.

The definition of the roughness index (Definition 3) is not convenient for estimation based on discrete observations, as it involves checking the finiteness of an asymptotic limit and does not have an obvious finite sample analogue. In the next sections, we introduce a non-parametric estimator of the roughness index based on the concept of *normalized p -th variation*.

2.2 Normalized p -th variation

It is not easy to use p -th variation directly on empirical data for estimating roughness based on discrete observations, as this involves checking convergence to an unknown limit. We introduce a normalized version of p -th variation which has better asymptotic properties [10]:

Definition 4 (Normalized p -th variation along a sequence of partitions). *Let π be a sequence of partitions of $[0, T]$ with mesh $|\pi^n| \rightarrow 0$ and $\pi^n = (0 = t_1^n < t_2^n < \dots < t_{N(\pi^n)}^n = T)$. $x \in V_\pi^p([0, T], \mathbb{R})$ is said to have normalized p -th variation along π if there exists a continuous function $w(x, p, \pi) : [0, T] \rightarrow \mathbb{R}$ such that:*

$$\forall t \in [0, T], \quad \sum_{\pi^n \cap [0, t]} \frac{|x(t_{i+1}^n) - x(t_i^n)|^p}{[x]_\pi^{(p)}(t_{i+1}^n) - [x]_\pi^{(p)}(t_i^n)} \times (t_{i+1}^n - t_i^n) \xrightarrow{n \rightarrow \infty} w(x, p, \pi)(t). \quad (5)$$

We denote $N_\pi^p([0, T], \mathbb{R})$ the class of all continuous functions for which the normalized p -th variation² exists.

The terminology is justified by the following result [10] which shows that, for a large class of functions with p -th variation, the normalized p -th variation exists and is linear:

²For $p = 2$ we will call this quantity as 'normalized quadratic variation'.

Theorem 2.3. Let $x \in V_\pi^p([0, T], \mathbb{R})$ for some $p > 1$ where π be a sequence of partitions of $[0, T]$ with vanishing mesh $|\pi^n| \rightarrow 0$. Furthermore, if the p -th variation is absolutely continuous then:

$$x \in N_\pi^p([0, T], \mathbb{R}) \quad \text{and} \quad \forall t \in [0, T], w(x, p, \pi)(t) = t.$$

Proof. See Appendix. □

The following result shows that normalized p -th variation is a ‘sharp’ statistic: if a function has finite p -th variation along a sequence of partitions π then for all $q \neq p$ the normalized p -th variation is either infinite or zero.

Theorem 2.4. Let π be a sequence of partitions of $[0, T]$ with mesh $|\pi^n| \rightarrow 0$. Let $x \in V_\pi^p([0, T], \mathbb{R})$ with $[x]_\pi^{(p)} \in (0, \infty)$ for some $p > 1$.

- (i) For all $t \in (0, T]$ and for all $q > p$; $w(x, q, \pi)(t) = \infty$.
- (ii) For all $t \in [0, T]$ and for all $q < p$; $w(x, q, \pi)(t) = 0$.

Proof. The proof is provided in Appendix. □

In particular, Brownian motion almost surely has linear normalized quadratic variation.

Example 2 (Normalized quadratic variation for Brownian motion). Let B be a Wiener process on a probability space $(\Omega, \mathcal{F}, \mathbb{P})$, and $(\pi^n)_{n \geq 1}$ be a sequence of partitions of $[0, T]$ with $|\pi^n| \log n \rightarrow 0$. Then:

$$\mathbb{P}(w(B, 2, \pi)(t) = t) = 1.$$

Proof. The proof is provided in the Appendix. □

Remark 2. In the above example, instead of taking any partition sequence with $|\pi^n| \log n \rightarrow 0$, we can also take any refining sequence of partitions. The proof is then different and uses the martingale convergence theorem [10].

Example 3 (Stochastic integrals). Let $X(t) = \int_0^t \sigma(u) dB_u$ where σ is an adapted process with $\int_0^T \sigma^2(u) du < \infty$. Then, for any refining partition sequence π with vanishing mesh,

$$\mathbb{P}(w(X, 2, \pi)(t) = t) = 1.$$

Proof. This is an immediate consequence of Theorem 2.3. □

Remark 3. In the statement of Example 3, we can replace the assumption of refining partitions with partitions satisfying $|\pi^n| \log(n) \rightarrow 0$.

Example 4 (Normalized p -th variation for fractional Brownian motion). Let B^H be a fractional Brownian motion with Hurst index H , on a probability space $(\Omega, \mathcal{F}, \mathbb{P})$. B^H has normalized p -th variation along the dyadic partition $\mathbb{T} = (\mathbb{T}^n)_{n \geq 1}$ for $p = 1/H$ almost-surely:

$$\mathbb{P}\left(w\left(B^H, \frac{1}{H}, \mathbb{T}\right)(t) = t\right) = 1.$$

Proof. The proof is a consequence of [27, Proposition 4.1]. □

Schied and Mishura [23] have provided several examples of functions with prescribed p -th variation. The class of functions \mathcal{X}^p defined in [23] is described as follows:

$$\mathcal{X}^p = \left\{ x \in C^0([0, 1], \mathbb{R}) \mid x(t) = \sum_{m=0}^{\infty} 2^{m(\frac{1}{2} - \frac{1}{p})} \sum_{k=0}^{2^m-1} \theta_{m,k} e_{m,k}(t), \theta_{m,k} \in \{-1, +1\} \right\}. \quad (6)$$

The graph of $e_{m,k}$ is a wedge with height $2^{-\frac{m+2}{2}}$, width 2^{-m} , centred at $c_{m,k} = 2^{\frac{k-1}{2^m}}$. In particular, the functions $e_{m,k}, e_{m,k'}$ have disjoint support for $k' \neq k$.

Example 5. Any function $x \in \mathcal{X}^p$ possesses normalized p -th variation along the dyadic partition sequence \mathbb{T} and

$$\forall x \in \mathcal{X}^p, \forall t \in [0, 1], \quad w(x, p, \mathbb{T})(t) = t.$$

Proof. The proof is provided in the Appendix. \square

2.3 Estimating roughness from discrete observations

Given observations on a refining time partition π^L , we define the ‘normalized p -th variation statistic’ which is the discrete counterpart of the normalized p -th variation:

$$W(L, K, \pi, p, t, X) := \sum_{\pi^K \cap [0, t]} \frac{|X(t_{i+1}^K) - X(t_i^K)|^p}{\sum_{\pi^L \cap [t_i^K, t_{i+1}^K]} |X(t_{j+1}^L) - X(t_j^L)|^p} \times (t_{i+1}^K - t_i^K). \quad (7)$$

The definition of the statistic (7) involves two frequencies: a ‘block’ frequency K and a sampling frequency $L \gg K$. As the partition is refining, π^K is a subpartition of π^L . The denominator is estimated by grouping the sample of size L into K many groups, where each group contains $\frac{L}{K}$ consecutive data points.

The statistic (7) converges to the normalized p -th variation (5) as the sampling frequency L and block frequency increase:

$$\lim_{K \rightarrow \infty} \lim_{L \rightarrow \infty} W(L, K, \pi, p, t, x) = w(x, p, \pi)(t).$$

It is thus natural to define roughness estimators for a discretely sampled signal in terms of (7).

The *variation index estimator* $\hat{p}_{L,K}^\pi(X)$ associated with the signal sampled on π^L is then obtained by computing $W(L, K, \pi, p, t, X)$ for different values of p and solving the following equation for $p_{L,K}^\pi(X)$,

$$W(L, K, \pi, \hat{p}_{L,K}^\pi(X), T, X) = T. \quad (8)$$

One can either fix a window length T or solve (8) in a least squares sense across several values of T .

An estimator for the roughness index is subsequently defined as:

$$\hat{H}_{L,K}^\pi(X) = \frac{1}{\hat{p}_{L,K}^\pi(X)}. \quad (9)$$

We will denote the roughness estimator (9) as $\hat{H}_{L,K}$ when the underline dataset and the corresponding partition sequence are clear. Asymptotic properties of these estimators under high-frequency sampling are studied in [10].

2.4 Finite sample behaviour of the roughness estimator

We will now study the finite sample behaviour of the roughness estimator $\hat{H}_{L,K}^\pi(X)$ using high-frequency simulations of fractional Brownian motions. In the simulation examples unless mentioned otherwise we will use a uniform partition sequence of $[0, 1]$ with:

$$\pi^n = \left(0 < \frac{1}{n} < \frac{2}{n} < \cdots < 1 \right).$$

To assess the finite sample accuracy of the estimator we compare the roughness index estimator $\hat{H}_{L,K}^\pi$ with the underlying Hurst exponent $H \in \{0.1, 0.3, 0.5, 0.8\}$. For every simulated path

we compute $W(L = 300 \times 300, K = 300, \pi, q, t = 1, X = B^H)$ for different values of q , in order to estimate $\hat{H}_{L,K}$. In figure 1, the black line is the value of $\log(W(L = 300 \times 300, K = 300, \pi, q = p, t = 1, X = B^H))$ plotted against roughness index $1/p$. The blue horizontal line represents the estimated roughness index $\hat{H}_{L,K}$ whereas the dotted horizontal line represents the Hurst parameter. Figure 2 shows the histograms of the estimator $\hat{H}_{L,K}^\pi$ generated from 150 independent paths. We observe that for datasets with length $L = 300 \times 300$ our roughness estimator $\hat{H}_{L=300 \times 300, K=300}$ has satisfactory accuracy. Table 2 provides summary statistics for roughness index \hat{H} of simulated fractional Brownian motions. Figure 3 represents a similar plot for simulated fractional Brownian motion with Hurst parameter $H = 0.1$. In Figure 3, in left, similar to Figure 1, $\log(W(L = 2000 \times 2000, K = 2000, \pi, p, t = 1, X = B^H))$ is plotted against $H = 1/p$ and the right plot represents the histograms of the estimator $\hat{H}_{L=2000 \times 2000, K=2000}$. The summary statistics for the estimator are provided in Table 2. To compute the estimator $\hat{H}_{L,K}$ we have different possible choices of $K \ll L$. Figure 4 shows how the estimator $\hat{H}_{L,K}^\pi$ varies with K for fractional Brownian motion with Hurst parameter $H = 0.1$. The black line represents the $\hat{H}_{L,K}$ plotted against different values of K whereas the blue vertical line represents the value for $L = 300 \times 300, K = 300$. We observe that when we vary K in the neighbourhood $K \approx \sqrt{L}$ the estimator performs reasonably well and is not very sensitive to the choice of K in this vicinity.

In summary, we observe that for realistic sample sizes and frequencies encountered in high-frequency financial data, the estimator is quite accurate and not sensitive to the block size K in the range $K \approx \sqrt{L}$.

H	Min.	Lower quartile	Median	Mean	Upper quartile	Max.
0.1	0.0650	0.0920	0.1030	0.1009	0.1100	0.1440
0.3	0.2730	0.2940	0.2980	0.2976	0.3020	0.3180
0.5	0.4820	0.4940	0.4980	0.4978	0.5020	0.5140
0.8	0.7570	0.7820	0.7900	0.7891	0.7940	0.8220

Table 1: Summary statistics for estimated roughness index $\hat{H}_{L,K}$ for fractional Brownian motion B^H with $L = 300 \times 300, K = 300$.

Hurst index H	Min.	Lower quartile	Median	Mean	Upper quartile	Max.
0.1	0.086	0.096	0.099	0.099	0.103	0.117

Table 2: Summary statistics for estimated roughness index $\hat{H}_{L,K}$ for fractional Brownian motion B^H with $H = 0.1, L = 2000 \times 2000, K = 2000$.

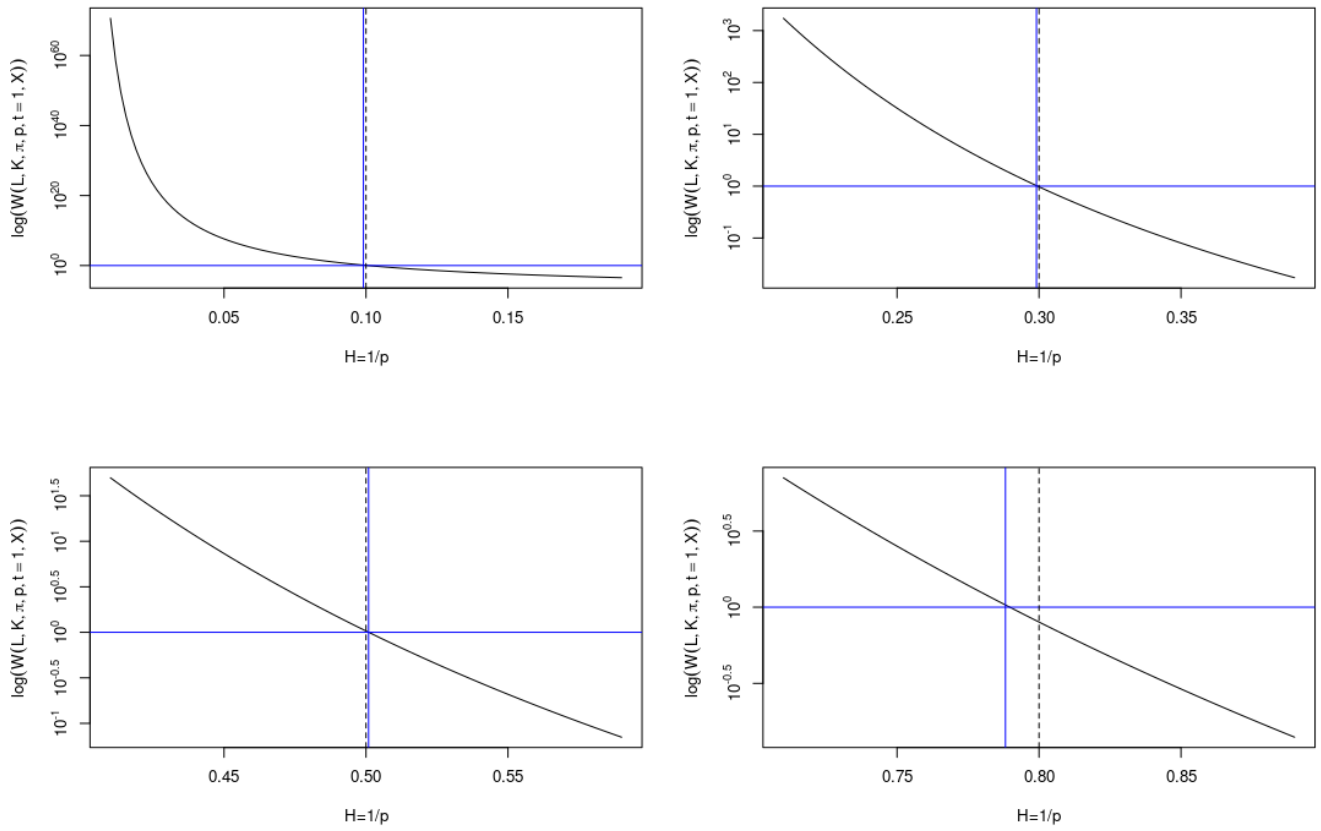


Figure 1: Logarithm of the normalized p -variation statistic for fractional Brownian motion with Hurst parameter $H \in \{0.1, 0.3, 0.5, 0.8\}$. The black solid line represents the log of normalized p -th variation statistics plotted against $H = 1/p$. The blue vertical line represents $\hat{H}_{L,K}$ using the normalized p -th variation statistics (with $L = 300 \times 300, K = 300$). The horizontal dotted line represents the true Hurst parameter H .

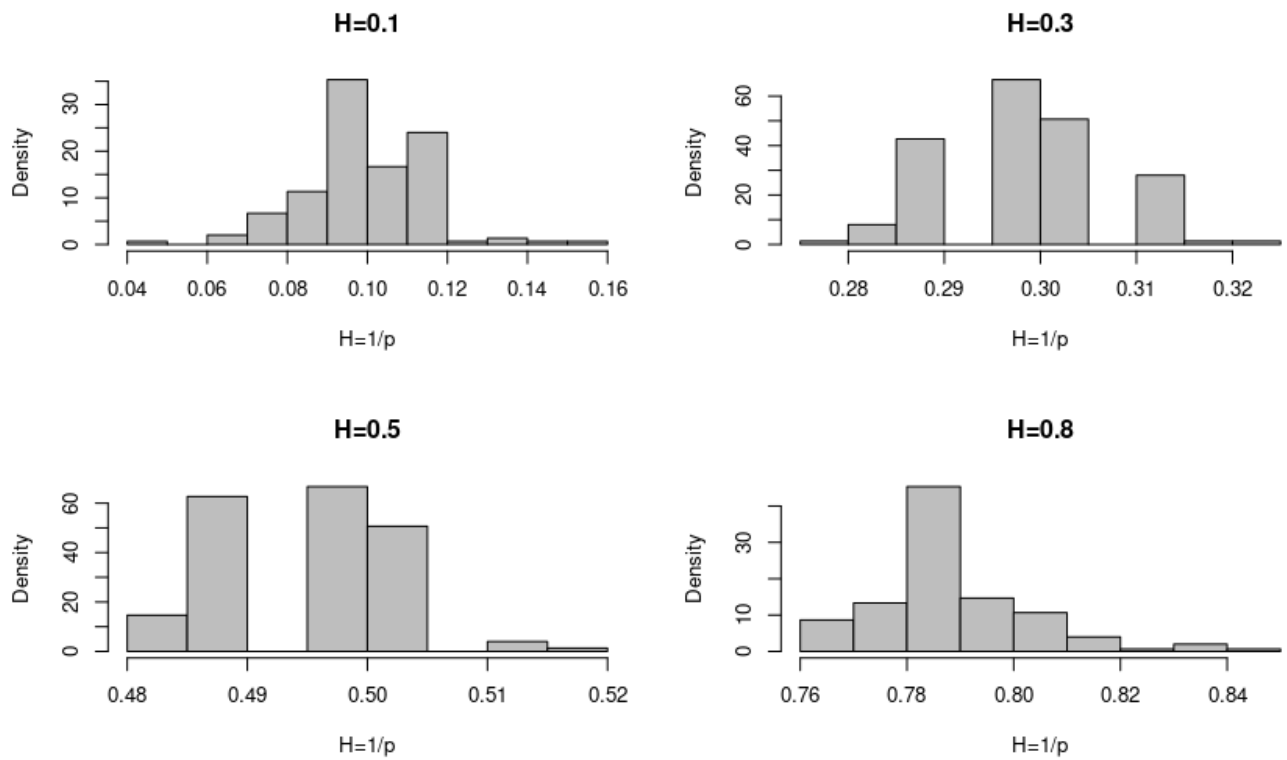


Figure 2: Histogram of estimated roughness index $\hat{H}_{L,K}$ with $L = 300 \times 300, K = 300$ generated from 150 independent simulations of fractional Brownian motion with Hurst parameter $H \in \{0.1, 0.3, 0.5, 0.8\}$.

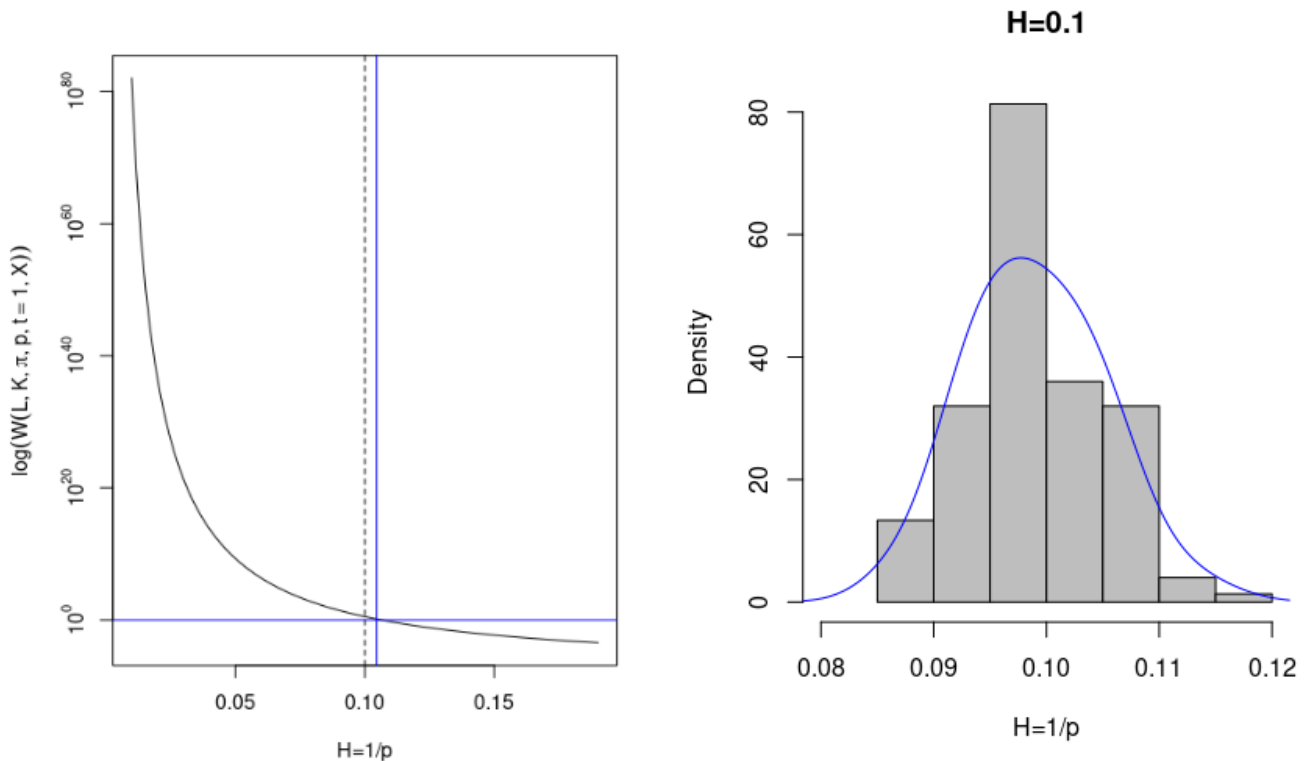


Figure 3: Simulation results for fractional Brownian motion with Hurst parameter $H = 0.1$. **Left:** The log of normalized p -th variation statistic is plotted against $H = 1/p$ in black. The blue vertical line represents the estimated roughness index $\hat{H}_{L,K}$ (with $L = 2000 \times 2000$, $K = 2000$), whereas the dotted line represents the true value $H = 0.1$. **Right:** Histogram of estimated roughness index $\hat{H}_{L,K}$ generated by simulating $n = 150$ independent fractional Brownian paths with Hurst parameter $H = 0.1$. The blue line represents a kernel estimator for the density.

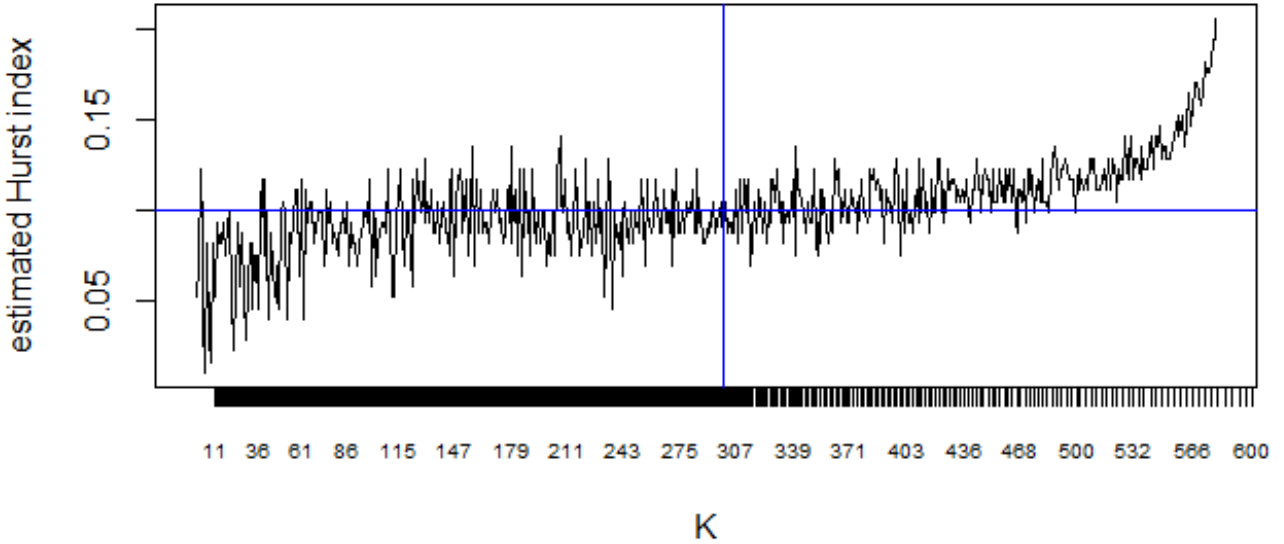


Figure 4: The solid black line represents the estimated roughness index $\hat{H}_{L=300 \times 300, K}$ plotted against different values of K for a fractional Brownian motion with Hurst parameter $H = 0.1$. The blue vertical line represents for $L = 300 \times 300, K = 300$ whereas the blue horizontal line represents the true value $H = 0.1$.

3 Spot volatility and realized volatility

Contrary to prices of an asset which may be observed and sampled directly from market data, (*spot*) *volatility* is not directly observable and as a consequence must be estimated from prices. Stochastic volatility models represent the price of a financial asset as the solution of a stochastic differential equation driven by a Brownian motion:

$$dS_t = \sigma_t S_t dB_t + \mu_t S_t dt \quad (10)$$

where the coefficient σ_t represents the instantaneous or ‘spot’ volatility. In general, σ_t is represented as a random process itself driven by fractional processes.

In a practical situation, the price S_t at time t , is usually observed over a non-uniform time grids of $[0, T]$:

$$\pi^n = \left(0 = t_0^n < t_1^n < \cdots < t_{N(\pi^n)}^n = T \right). \quad (11)$$

In order to study high-frequency asymptotics of roughness estimators, we assume $|\pi^n| \rightarrow 0$ as n increases; here the index n may be thought of as a ‘sampling frequency’. An example to keep in mind is the dyadic partition sequence: $\pi^n = (t_i^n = \frac{iT}{2^n}, i = 0, \dots, 2^n)$ but none of the results below requires a uniform grid.

The spot volatility process σ_t may then be recovered from the *quadratic variation* of the log-price $X = \log S$ along this particular grid:

$$\sigma_t^2 = \frac{d}{dt} [\log S]_\pi(t) \quad (12)$$

where the quadratic variation $[\log S]_\pi$ of the log-price

$$[\log S]_\pi(t) = \lim_{n \rightarrow \infty} \sum_{\pi^n \cap [0, t]} \left(\log \frac{S(t_{i+1}^n)}{S(t_i^n)} \right)^2 = \lim_{n \rightarrow \infty} RV_t(\pi^n)^2$$

is computed as a high-frequency limit of the *realized variance* [3, 1] along the sampling grid π^n , defined as

$$RV_t(\pi^n)^2 = \sum_{\pi^n \cap [0, t]} \left(\log \frac{S(t_{i+1}^n)}{S(t_i^n)} \right)^2 = \sum_{\pi^n \cap [0, t]} (X(t_{i+1}^n) - X(t_i^n))^2. \quad (13)$$

The realized volatility is defined as the square root of the realized variance.

Definition 5 (Realized volatility). *The realized volatility of a price process S over time interval $[t, t + \delta]$ sampled along the time partition π^n is defined as:*

$$RV_{t, t+\Delta}(\pi^n) = \sqrt{\sum_{\pi^n \cap [t, t+\Delta]} (X(t_{i+1}^n) - X(t_i^n))^2} = \sqrt{[X]_{\pi^n}(t + \Delta) - [X]_{\pi^n}(t)} \quad (14)$$

where $X = \log S$.

If the price S_t follows a stochastic volatility model (10) with **instantaneous volatility** σ_t then realized variance converges to the quadratic variation of $\log S$ (also called ‘*integrated variance*’) as sampling frequency increases [3, 19]:

$$RV_t(\pi^n)^2 \xrightarrow[n \rightarrow \infty]{\mathbb{P}} IV_t := \int_0^t \sigma_u^2 du, \quad RV_{t, t+\Delta}(\pi^n) \xrightarrow[n \rightarrow \infty]{\mathbb{P}} \sqrt{IV_{t, t+\Delta}} = \sqrt{\int_t^{t+\Delta} \sigma_u^2 du}. \quad (15)$$

Along a single price path observed at high-frequency, we can compute the realized variance (14) and the realized volatility $RV_{t, t+\Delta}(\pi^n)$ in (15) may be used as a practical indicator of volatility:

$$RV_{t, t+\Delta}(\pi^n) \simeq \sqrt{\Delta} \sigma_t.$$

Several empirical studies have attempted to estimate the roughness of ‘realized volatility’ signals using high-frequency data [1, 3, 11, 19, 24]. A well-known reference is the study of Gatheral et al. [16] where the authors estimate the roughness index of S&P500 realized volatility by performing the following logarithmic regression to :

$$m(q, \Delta) = \frac{1}{n} [\log RV]_{\pi^n}^{(q)} = \frac{1}{n} \sum_{t=1}^n |\log(RV_{t+\Delta}) - \log(RV_t)|^q \approx C_q \Delta^{\xi_q}. \quad (16)$$

The coefficients ξ_q are also shown to behave linearly in q :

$$\xi_q \approx q \widehat{H}_R.$$

Regression of ξ_q on q yields an estimate \widehat{H}_R of Hurst/Hölder index, for which Gatheral et al [16] report the value $\widehat{H}_R = 0.13$. Based on these observations, they propose a fractional SDE for (spot) volatility:

$$d \log \sigma_t^2 = \mu_t dt + \eta dB_t^H.$$

As we see from Equation 16, the method used in [15] actually uses p -th variation of the $\log(RV)$ to calculate the roughness of the underlying volatility process. Figure 5 is a replication of the log-regression model described above to estimate the roughness index of the volatility of 5-min

S&P 500. However, in an interesting simulation study using paths simulated from a Brownian OU volatility process, Rogers [25] showed that the scaling behavior claimed as evidence for ‘rough volatility’ is also observed in a Brownian OU model over a range of time scales, and that estimators of the roughness index based on log-regression of empirical p -th variation have poor accuracy.

Similar evidence for the lack of accuracy of such estimators based on linear-regression of p -th variation is shown by Fukasawa et al. [14].

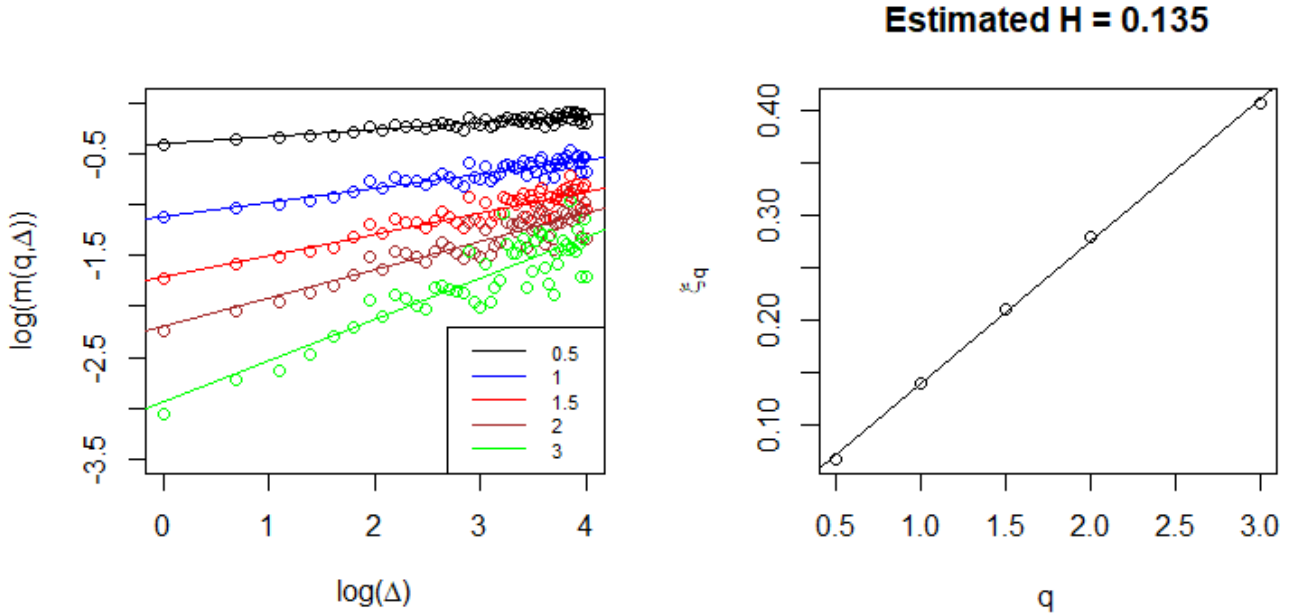


Figure 5: **Left:** A reproduction of the linear-regression method introduced by Gatheral et al. [16] using SPX 5-minute realized volatility from the Oxford-Man Institute’s Realized Library. **Right:** Regression of ξ_q vs q : the estimated slope is $\widehat{H}_R = 0.135$.

4 Simulation experiments

We now compare various estimators of the roughness index for instantaneous volatility σ_t with those obtained from realized volatility $RV_{t,t+\Delta}(\pi^n)$ using price trajectories simulated from stochastic volatility models with varying degrees of “roughness”.

4.1 Stochastic volatility diffusion models

Let us first consider the following stochastic volatility where volatility is simply (the modulus of) a Brownian motion:

Example 6.

$$dS_t = \sigma_t S_t dB_t, \quad \text{with} \quad \sigma_t = |W_t|, \quad (17)$$

where B, W are independent Brownian motions.

Figure 6 represents a path of the instantaneous volatility σ_t and the realized volatility $RV_t(\pi^L)$ computed as in Equation 14 by taking $L/K = 300$ consecutive data-points. The right plot of Figure 6 represents the microstructure noise, which is defined as the difference of instantaneous and realized volatility. The ACF of the microstructure noise shows a complex time-dependent pattern which rules out IID behavior and indicates a complex dependence structure.

The estimated roughness index of instantaneous and realized volatility are observed to be very different. In the left graph of Figure 7 we plot $\log(W(K = 500, L = 500 \times 500, \pi, p, t = 1, X = RV))$ against $H = 1/p$ for the realized volatility. On the other hand, the right graph is the same plot with the same set of parameters but for instantaneous volatility. The estimated roughness index for realized volatility ($\hat{H}_{L=500 \times 500, K=500}(RV) = 0.27$) is significantly smaller than the roughness index of the instantaneous volatility ($\hat{H}_{L=500 \times 500, K=500}(\sigma) = 0.49$) suggesting rougher behaviour of realized volatility. As in our simulation study we do not have any measurement errors, this roughness behaviour purely comes from microstructure noise. In some studies it is assumed that the microstructure noise is IID (see e.g. [14]) but as we can see from this diffusion example, the microstructure noise is far from IID.

The solid black lines in Figure 8 and Figure 9 respectively represent the estimated roughness index $\hat{H}_{L=300 \times 300, K}$ plotted against different values of K for the realized and instantaneous volatility (model 17). The blue vertical line represents for $K = 500, L = 500 \times 500$. From the figures, we can observe that irrespective of the choice of K for the finite sample dataset of length $L = 500 \times 500$, the realized volatility is significantly rougher than the instantaneous volatility.

We now compare our roughness estimator with the log-regression method used in Gatheral et al. [16] for the model 17. It turns out that even with the linear-regression model, similar ‘rougher’ realized volatility is observed even if the instantaneous volatility has Brownian diffusive behaviour. Figure 10 and Figure 11 show that the realized volatility has a significant smaller roughness index than the instantaneous volatility even with respect to the linear regression method. In this example it is clear that the roughness observed in realized volatility is attributable to the discretization error (‘microstructure noise’) and not the roughness of the spot volatility process, which is Brownian.

Next we consider a more realistic mean-reverting volatility model in which the volatility follows a Brownian Ornstein–Uhlenbeck process:

Example 7 (OU-SV model).

$$dS_t = S_t \sigma_t dB_t, \quad \sigma_t = \sigma_0 e^{Y_t}, \quad dY_t = -\gamma Y_t dt + \theta dB_t. \quad (18)$$

In the simulation, we use $\sigma_0 = 1, Y_0 = 0$ and $\gamma = \theta = 1$. The left plot of Figure 12 represents the realized volatility (respectively instantaneous volatility) of the price process in black (respectively red) simulated from the above stochastic volatility model 18. The right plot of Figure 12 represents the corresponding microstructure noise, which is the difference between the realized and the instantaneous volatility. Visually the plot suggests the microstructure noise has a complicated dependence structure, and the IID assumption for microstructure noise, as put forth for example in [14], is not very realistic.

Now we compare the distribution of the estimator $\hat{H}_{L,K}$ with $(L = 300 \times 300, K = 300)$ for realized and instantaneous volatility across 2500 independent paths drawn from (18). The left plot in Figure 13 is the distribution of $\hat{H}_{L,K}$ for the realized volatility while the right plot corresponds to the same for instantaneous volatility. The following table provides summary statistics for the estimator $\hat{H}_{L,K}$ with $L = 300 \times 300, K = 300$ across 2500 independent sample paths for realized volatility and instantaneous volatility respectively.

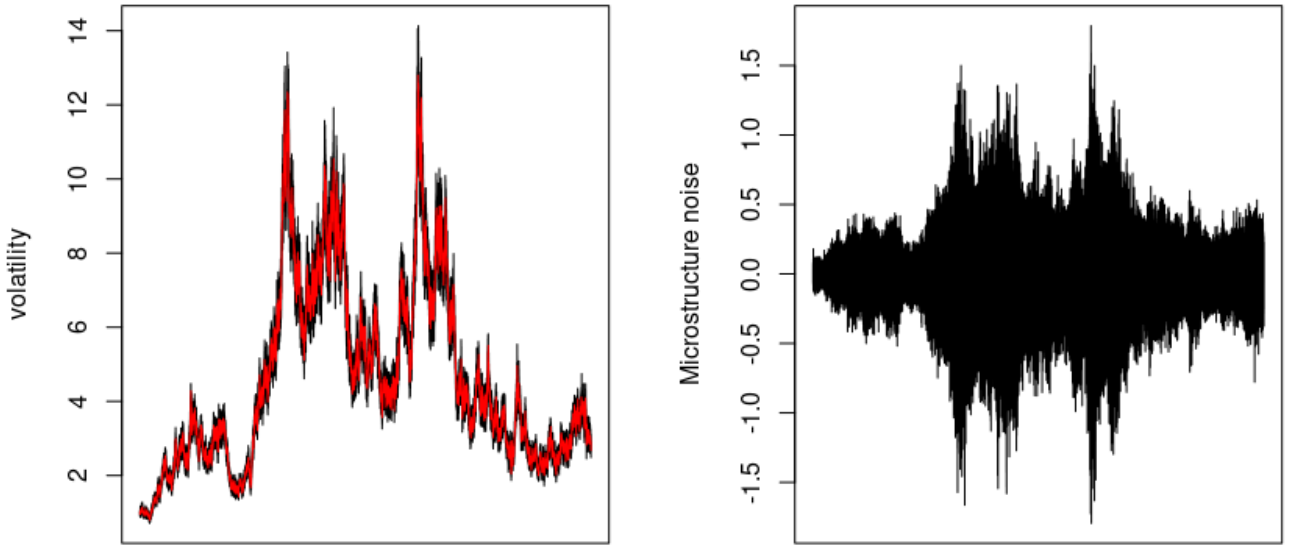


Figure 6: Simulation model: $\sigma_t = |B'_t|, dS_t = S_t \sigma_t dB_t$, where B_t and B'_t are Brownian motions independent of each other. **Left:** The red line represents instantaneous volatility σ_t whereas the black line represents realized volatility RV_t . **Right:** Corresponding microstructure noise for the left simulated path.

	Realized volatility	Instantaneous volatility
Min.	0.087	0.528
1st Quantile	0.128	0.552
Median	0.136	0.556
Mean	0.137	0.557
3rd Quantile	0.148	0.563
Max.	0.181	0.581

Table 3: Estimated roughness index $\hat{H}_{L,K}, L = 300 \times 300, K = 300$ for realized volatility and instantaneous volatility for the diffusion model (17) with $H = 0.5$.

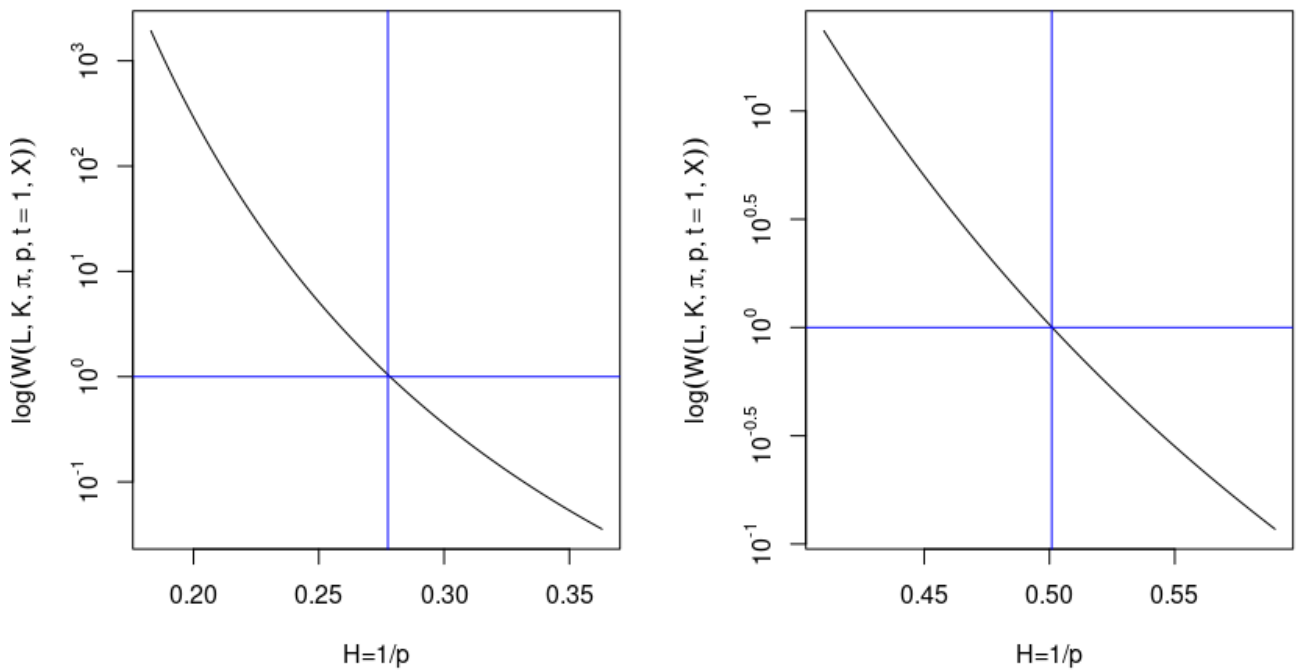


Figure 7: **Left:** Estimated roughness index $\hat{H}_{L,K}$ (via normalized p -variation statistic with $L = 500 \times 500, K = 500$), for realized volatility derived from a Brownian diffusion model, shown in Figure 6. **Right:** Estimated roughness index $\hat{H}_{L,K}$ for instantaneous volatility of the same price path.

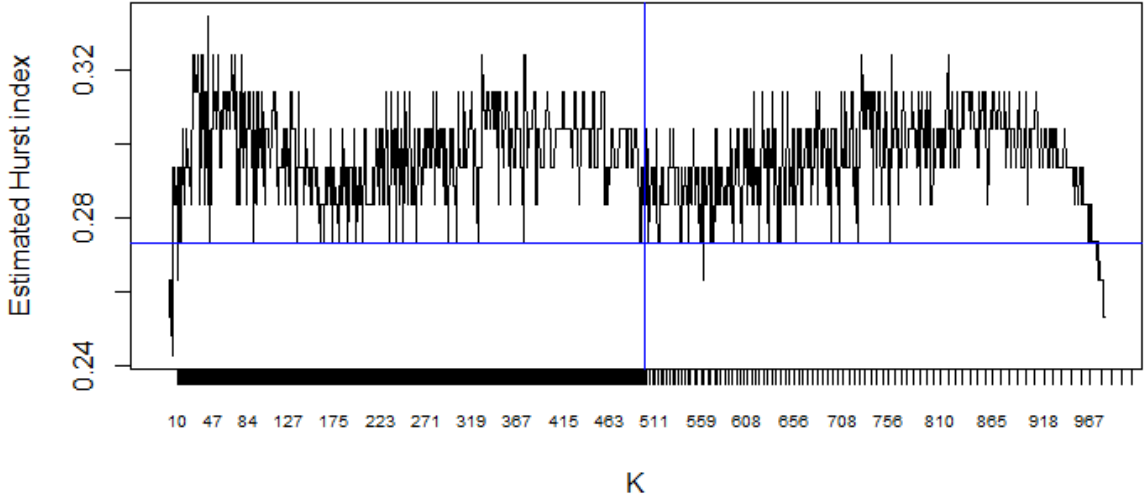


Figure 8: The solid black line represents the estimated roughness index $\hat{H}_{L,K}$ via normalized p -th variation statistic $W(L = 500 \times 500, K, \pi, q, t = 1, X = RV)$ plotted against different values of K for the realized volatility shown in Figure 6. The blue vertical line represents $L = 500 \times 500, K = 500$ whereas the blue horizontal line represents $\hat{H} = 0.273$.

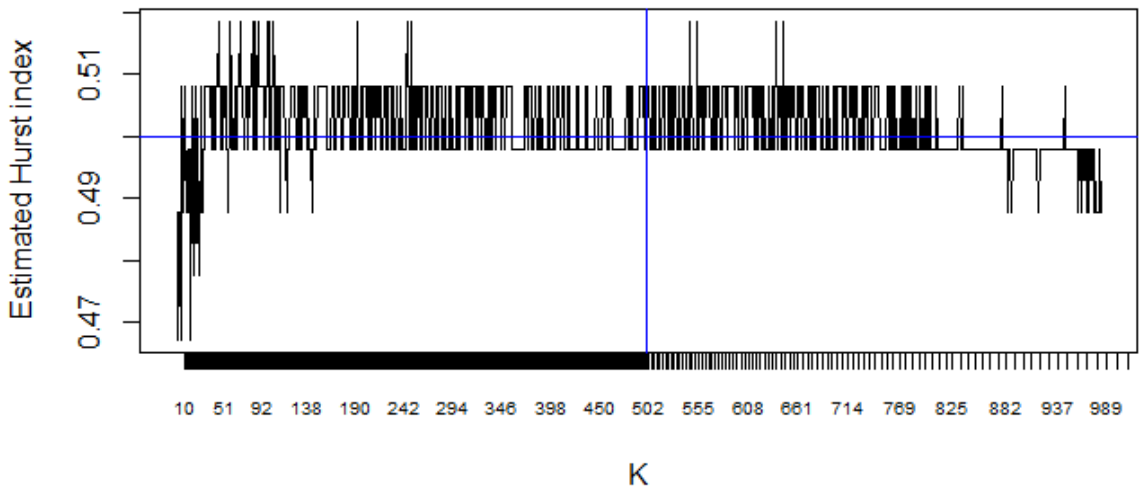


Figure 9: The solid black line represents the estimated roughness index $\hat{H}_{L,K}$ via normalized p -th variation statistic $W(L = 500 \times 500, K, \pi, q, t = 1, X = IV)$ plotted against different values of K for the instantaneous volatility shown in Figure 6. The blue vertical line represents $L = 500 \times 500, K = 500$ whereas the blue horizontal line represents true Hurst parameter $H = 0.5$.

Estimated $H = 0.499$

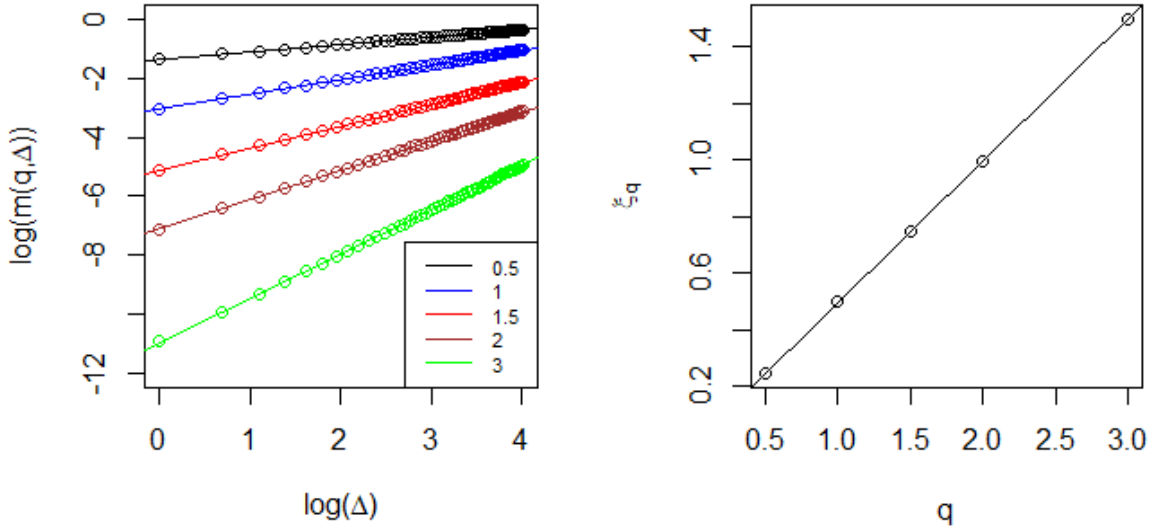


Figure 10: **Left:** Scaling analysis of instantaneous volatility of a simulated Brownian stochastic volatility model (Example 6) using the same log-regression method used by Gatheral et al. [16]. **Right:** regression coefficients ξ_q as a function of q . The estimated roughness index is $\widehat{H}_R = 0.499$.

Estimated $H = 0.342$

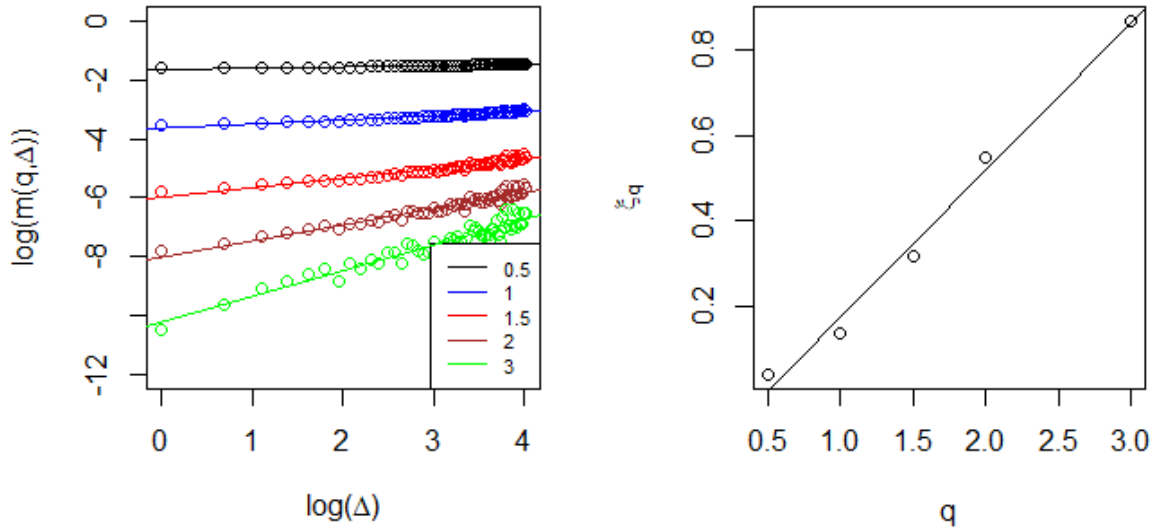


Figure 11: **Left:** Scaling analysis of realized volatility of a simulated Brownian stochastic volatility model (Example 6) using the same log-regression method used by Gatheral et al. [16]. **Right:** regression coefficients ξ_q as a function of q . The estimated roughness index is $\widehat{H}_R = 0.342$.

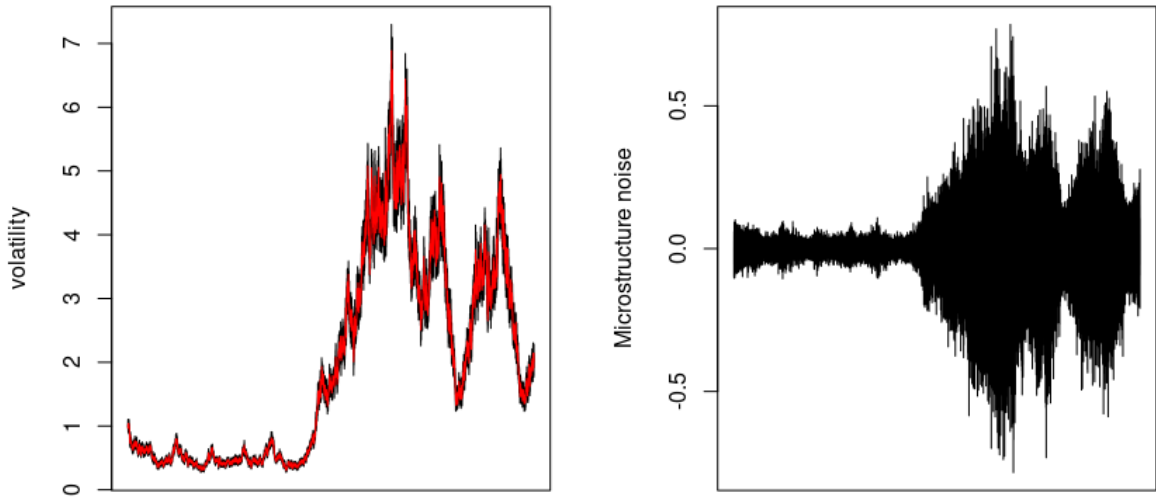


Figure 12: **Left:** Realized volatility (in black) vs instantaneous volatility (red) for the OU price model (18). **Right:** Microstructure noise.

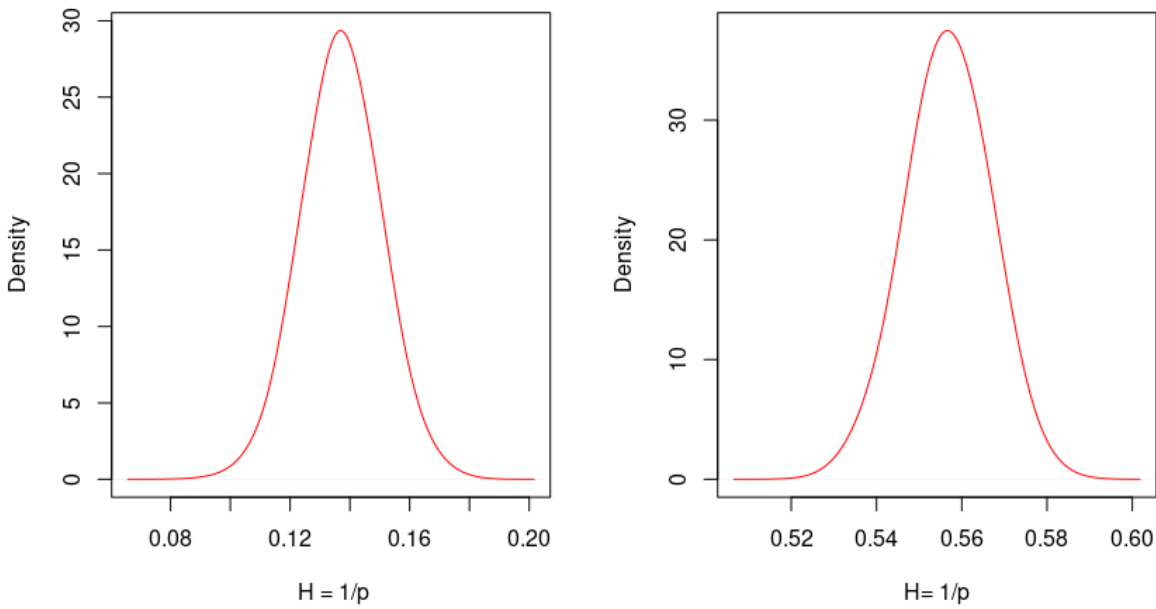


Figure 13: Distribution of the estimated roughness index $\hat{H}_{L,K}$ for $(L = 300 \times 300, K = 300)$ across 2500 independent simulations for the OU-SV model (18) with roughness index $H = 0.5$. **Left:** Realized volatility. **Right:** Instantaneous volatility.

4.2 A fractional Ornstein-Uhlenbeck model

In both previous examples, instantaneous volatility follows a diffusive behaviour similar to Brownian motion with $H = \frac{1}{2}$, yet the realized volatility exhibits "rough" behaviour with an estimated roughness index significantly smaller than 0.5.

We now consider the more general case of a price process generated by a stochastic volatility model of the type (1) where instantaneous volatility has a general roughness index $H \in (0, 1)$ and explore how the roughness index of the instantaneous volatility reflects on the roughness index of realized volatility and the corresponding microstructure noise.

Example 8. [Fractional OU process] Consider the following price process, where the volatility is described by a fractional Ornstein-Uhlenbeck process:

$$dS_t = \sigma_t S_t dB_t, \quad \sigma_t = \sigma_0 e^{Y_t}; \quad dY_t = -\gamma Y_t dt + \theta dB_t^H, \quad (19)$$

where $\gamma = \theta = \sigma_0 = 1$, B is a Brownian motion and B^H fractional Brownian motion with Hurst index $H \in (0, 1)$.

We compute the realized volatility and compare the estimated roughness index $\hat{H}_{L,K}$ (with, $L = 300 \times 300$, $K = 300$) of instantaneous and realized volatility in the following table.

H	Instantaneous volatility	Realized volatility
0.10	0.130	0.190
0.20	0.215	0.250
0.30	0.310	0.258
0.40	0.413	0.207
0.50	0.507	0.130
0.60	0.601	0.087
0.70	0.678	0.061
0.80	0.756	0.052

The corresponding pictures for price process, realized volatility and the instantaneous volatility from Model 19 with Hurst index $H = \{0.05, 0.1, 0.2, 0.3, 0.4, 0.5, 0.6, 0.7, 0.8\}$ respectively are presented in Figure 14. Visually we can observe that for smaller H , the instantaneous volatility is rougher than realized volatility but as we increase H the realized volatility shows significantly rougher behaviour than the instantaneous volatility. In Figure 15 for the simulated models in Figure 14, we plot the estimated roughness index $\hat{H}_{L,K}(RV)$ and $\hat{H}_{L,K}(\sigma)$ respectively in the red and blue line. Though the estimated roughness index of instantaneous volatility (represented in blue line) gives an accurate estimate of Hurst index H , the roughness index for realized volatility always stays below 0.3. In particular, when the instantaneous volatility exhibits smoother behaviour (corresponding to $H \geq 0.5$) the estimated roughness index of realized volatility turns out to be a poor estimate for the Hurst index.

Figure 16 shows the corresponding estimators $\hat{H}_{L,K}(RV)$ and $\hat{H}_{L,K}(\sigma)$ for 100 independent simulated price paths from (19). The bold black lines represent the mean across 100 independent simulations whereas the dotted lines represent the corresponding 25% and 75% confidence intervals. For the price process (19), no matter what the value of the Hurst exponent for instantaneous volatility, the roughness index of realized volatility $\hat{H}_{L,K}(RV)$ is always estimated to be between 0 to 0.3.

These examples illustrate our point: one *cannot draw the conclusion* that (spot) 'volatility is rough' i.e. reject the null hypothesis $H(\sigma) = 1/2$ just because realized volatility exhibits 'rough' behaviour with $\hat{H}_{L,K}(RV) < \frac{1}{2}$ or $\hat{H}_R < 1/2$, *even* when these estimators exhibit values well below 1/2.

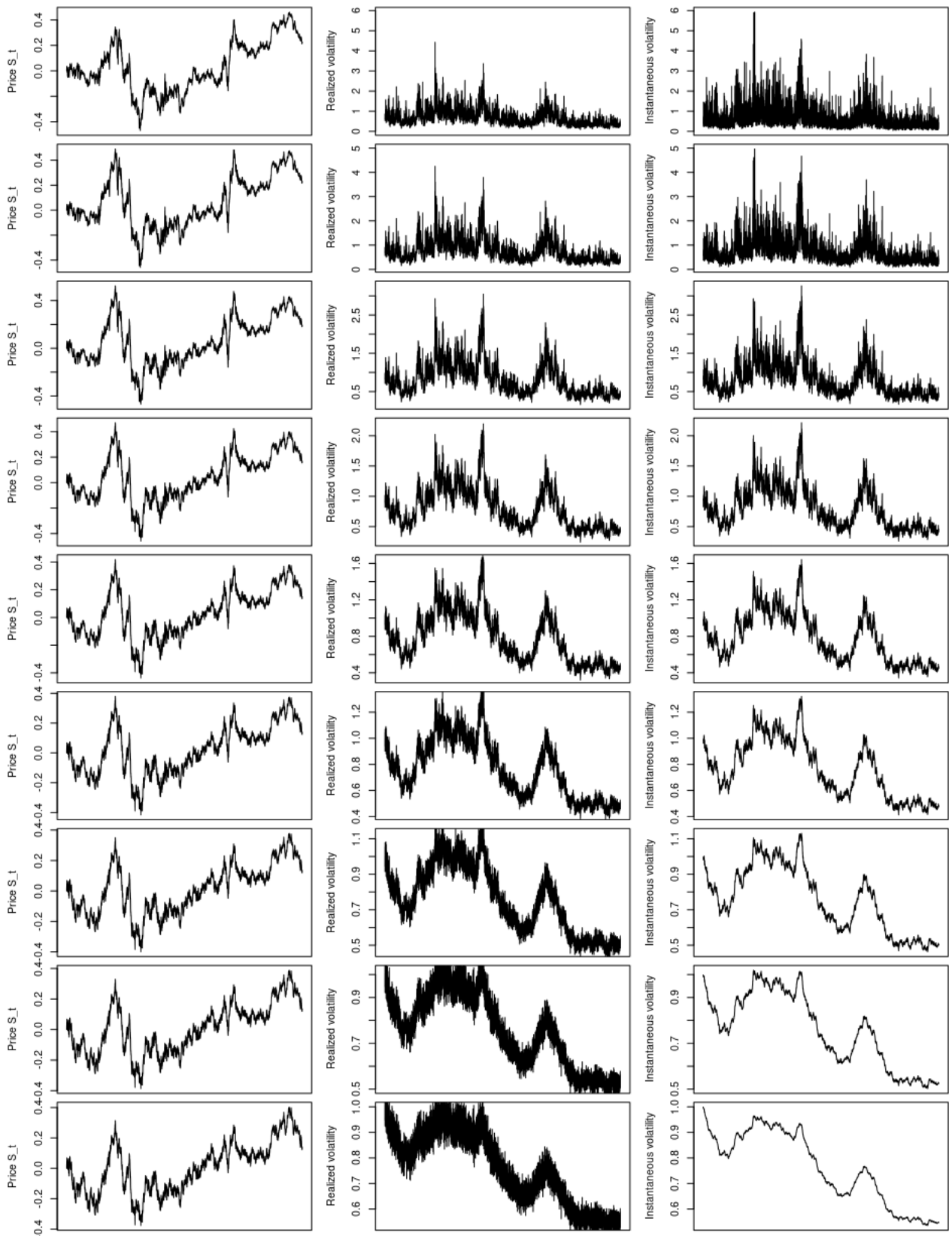


Figure 14: **Left:** Simulated price path S_t of fractional OU model (Equation 19) with $H=\{0.05, 0.1, 0.2, 0.3, 0.4, 0.5, 0.6, 0.7, 0.8\}$ respectively, **Center:** Realized volatility, **Right:** Instantaneous volatility.

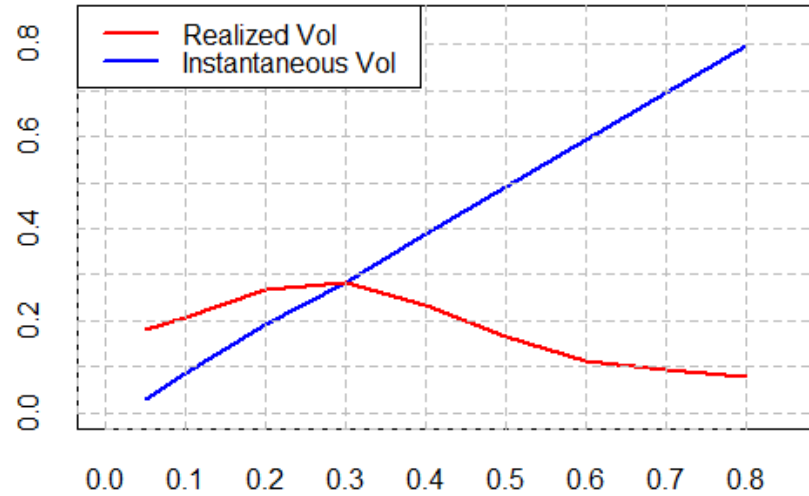


Figure 15: Estimated roughness index $\hat{H}_{L=300 \times 300, K=300}$ for realized volatility and instantaneous volatility from a high-frequency fractional-OU stochastic volatility model (Equation (19)), plotted for price path generated with different values of H .

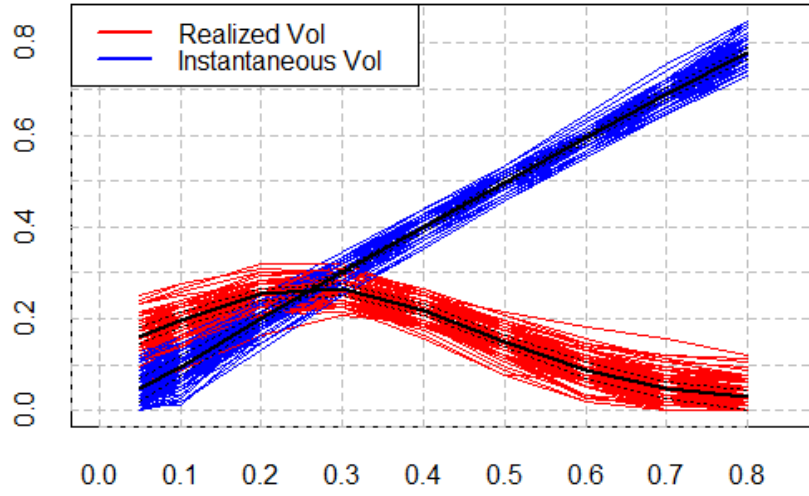


Figure 16: Estimated roughness index $\hat{H}_{L=300 \times 300, K=300}$ for realized volatility and instantaneous volatility for a high-frequency simulation of a fractional-OU stochastic volatility model (19), plotted against different Hurst index H for 100 independent price paths.

5 Application to high-frequency financial data

Having extensively explored the performance of our roughness estimator $\hat{H}_{L,K}$ based on the normalized p -th variation statistic for spot and realized volatility on simulated price paths, we now apply it to high-frequency financial time series.

5.1 AAPL

Figure 17 (left) shows the second-by-second record of AAPL stock price. The right graph of Figure 17 is $\log(W(L = 1900 \times 1900, K = 1900, \pi, p, t = 1, X))$ plotted against Hurst parameter $H = 1/p$ for ‘AAPL’ price.

The left plot of Figure 18 represents 1-minute realized volatility of ‘AAPL’ in 2016. The right graph of Figure 18 is $\log(W(L = 310 \times 310, K = 310, \pi, p, t = 1, X = RV))$ plotted against $H = 1/p$ for the 1-min AAPL realized volatility. Fixing the value of $L = 310 \times 310$, if we deviate the value of K a little, then the estimated roughness index varies between 0.08 to 0.22. This is consistent with the results of Gatheral et al. [16] regarding realized volatility. But as our simulation study suggests, the roughness index of realized volatility may be very different from that of spot volatility which is the quantity modelled in continuous-time stochastic volatility models.

5.2 SP500

Several studies on rough volatility, including the original study [16], are based on the Oxford-Man institute Realized Volatility dataset ³. Figure 19 represents the plot of 5-minute realized volatility of SP500. The X-axis represents date. The right graph of Figure 19 is $\log(W(L = 70 \times 70, K = 70, \pi, p, t = 1, X = RV))$ plotted against Hurst parameter $H = 1/p$ for the 5-min Oxford-Man institute realized volatility data. Fixing the value of $L = 70 \times 70$, if we deviate the value of K a little, the estimated roughness index $\hat{H}_{L,K}$ varies between 0.05 to 0.25. This finding is consistent with Gatheral’s findings [16].

Overall, the picture that emerges from SP500 and AAPL data is quite similar to the one observed in simulations of diffusion-type stochastic volatility models discussed in Section 4.1. As observed in Section 2.4, these observations are fully compatible with a diffusion-type stochastic volatility model such as (18) and one cannot reject the null hypothesis $H(\sigma) = 1/2$ just because realized volatility exhibits ‘rough’ behaviour with $\hat{H}_{L,K}(RV) < \frac{1}{2}$ or $\widehat{H}_R < 1/2$, even though these estimators exhibit values around 0.1.

³<https://realized.oxford-man.ox.ac.uk/data>

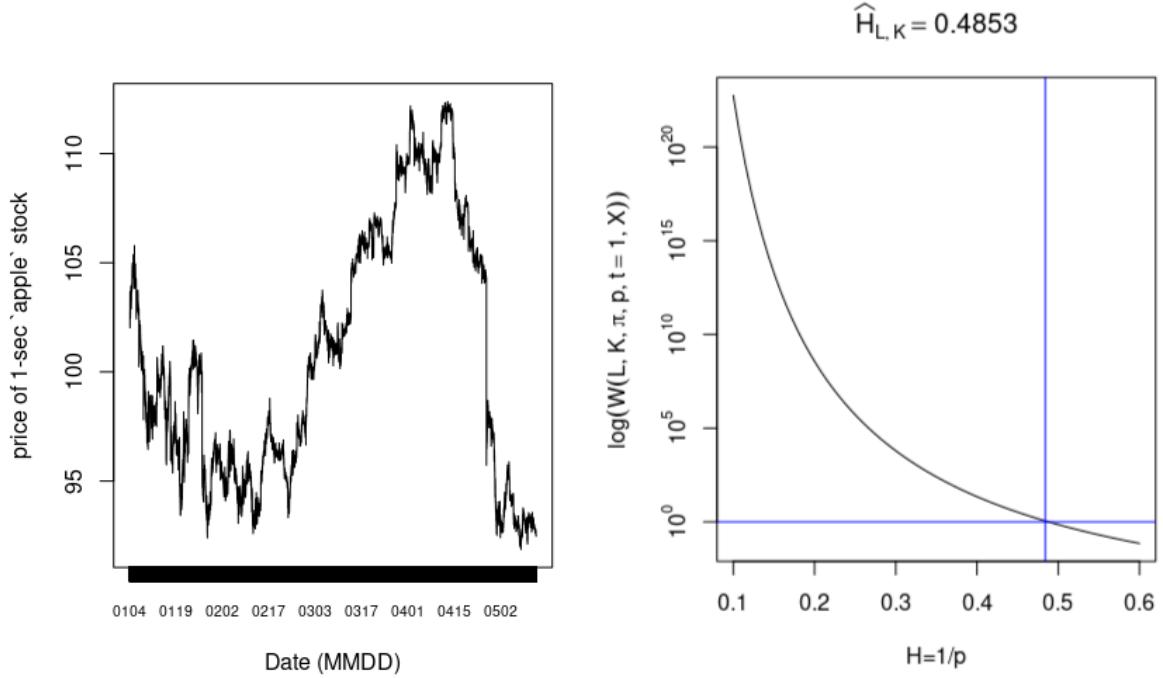


Figure 17: **Left:** price of AAPL 04/Jan/2016 - 11/May/2016 (90 days). **Right:** Roughness index estimator $\hat{H}_{L,K}$ (with $L = 1400 \times 1400$, $K = 1400$) for AAPL stock price data.

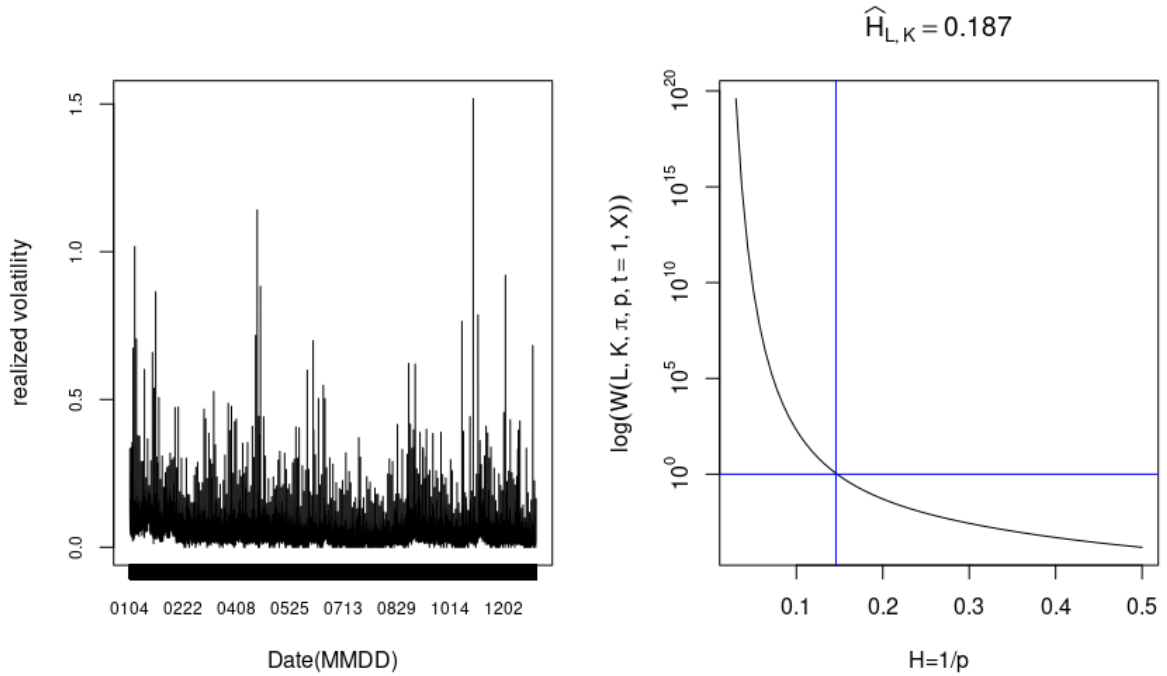


Figure 18: **Left:** Plot of 1-min realized volatility of 'AAPL' (year 2016). **Right:** Estimated roughness index $\hat{H}_{L,K}$ (with $L = 310 \times 310$, $K = 310$) for the 1-min realized volatility (estimated roughness index $\hat{H}_{L,K} \in [.08 - .22]$).

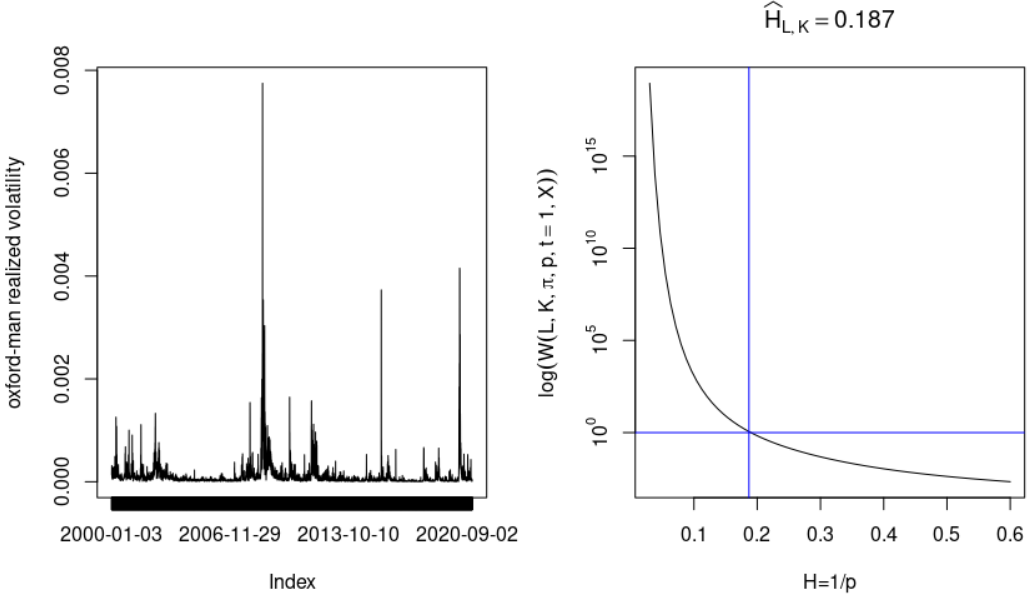


Figure 19: **Left:** S&P500 5-min realized volatility. **Right:** Estimated roughness index $\widehat{H}_{L,K} \in [.05 - .25]$ with $L = 70 \times 70, K = 70$.

6 Rough volatility ... or microstructure noise?

Given the large literature on ‘rough volatility’ in quantitative finance, it is somewhat surprising that the initial claim [16] that one needs to model the spot volatility process using a ‘rough’ fractional noise with Hurst exponent $H < 1/2$ has not been examined more closely, especially given that several follow-up studies [14, 25] point to the fact that the observations in [16] may well be compatible with a Brownian diffusion model for volatility.

Our detailed examples illustrate that, for stochastic-volatility diffusion models driven by Brownian motion as described in Examples 6 and 7, the realized volatility has a roughness index $\widehat{H}_{L,K} \approx 0.3$ so exhibits an ‘apparent roughness’ which instantaneous volatility does not have, both in terms of normalized p -th variation statistics and also in terms of the linear-regression method used by Gatheral et al. [16]. Clearly in these simulation examples this is entirely due to the discretization error or ‘microstructure noise’.

These results suggest that one cannot hastily conclude that the roughness observed in realized volatility is an indicator of similar behaviour in spot volatility, as implicitly assumed in the ‘rough volatility’ literature; the observations in high-frequency financial data are in fact compatible with a stochastic volatility model driven by Brownian motion and the origin of this apparent roughness may very well lie in microstructure noise rather than the noise process driving spot volatility.

Also, as shown in Example 8, the rough behaviour of realized volatility does not lead us to reject the hypothesis that the underlying spot volatility may be modelled with a Brownian diffusion model or even a smoother model with long-range dependence and $H > 1/2$. This observation, together with “Occam’s razor”, pleads for the use of Markovian stochastic volatility models which seem compatible with the empirical evidence but are far more tractable.

We are thus drawn to concur with Rogers [25] that “the notion that volatility is rough, that is, governed by a fractional Brownian motion (with $H < 1/2$), is not an incontrovertible established fact; simpler models explain the observations just as well.”

References

- [1] T. G. ANDERSEN, T. BOLLERSLEV, F. X. DIEBOLD, AND P. LABYS, *Modeling and forecasting realized volatility*, *Econometrica*, 71 (2003), pp. 579–625.
- [2] R. T. BAILLIE, T. BOLLERSLEV, AND H. O. MIKKELSEN, *Fractionally integrated generalized autoregressive conditional heteroskedasticity*, *Journal of Econometrics*, 74 (1996), pp. 3–30.
- [3] O. E. BARNDORFF-NIELSEN AND N. SHEPHARD, *Econometric analysis of realized volatility and its use in estimating stochastic volatility models*, *Journal of the Royal Statistical Society: Series B (Statistical Methodology)*, 64 (2002), pp. 253–280.
- [4] J. BERAN, *Statistics for long-memory processes*, vol. 61 of *Monographs on Statistics and Applied Probability*, Chapman and Hall, New York, 1994.
- [5] T. BOLLERSLEV AND H. OLE MIKKELSEN, *Modeling and pricing long memory in stock market volatility*, *Journal of Econometrics*, 73 (1996), pp. 151–184.
- [6] F. BREIDT, N. CRATO, AND P. DE LIMA, *The detection and estimation of long memory in stochastic volatility*, *Journal of Econometrics*, 83 (1998), pp. 325–348.
- [7] F. COMTE AND É. RENAULT, *Long memory in continuous-time stochastic volatility models*, *Mathematical Finance*, 8 (1998), pp. 291–323.
- [8] R. CONT, *Long range dependence in financial markets*, in *Fractals in Engineering*, J. Lévy-Véhel and E. Lutton, eds., London, 2005, Springer London, pp. 159–179.
- [9] ——, *Volatility clustering in financial markets: Empirical facts and agent-based models*, in Teyssière, Gilles and Kirman, Alan P. (eds.): *Long Memory in Economics*, Springer, Berlin, Heidelberg, 2007, pp. 289–309.
- [10] R. CONT AND P. DAS, *Measuring the roughness of a signal*, Working Paper, (2022).
- [11] R. CONT AND C. MANCINI, *Nonparametric tests for pathwise properties of semimartingales*, *Bernoulli*, 17 (2011), pp. 781 – 813.
- [12] R. CONT AND N. PERKOWSKI, *Pathwise integration and change of variable formulas for continuous paths with arbitrary regularity*, *Transactions of the American Mathematical Society*, 6 (2019), pp. 134–138.
- [13] R. M. DUDLEY, *Sample functions of the gaussian process*, *Ann. Probab.*, 1 (1973), pp. 66–103.
- [14] M. FUKASAWA, T. TAKABATAKE, AND R. WESTPHAL, *Consistent estimation for fractional stochastic volatility model under high-frequency asymptotics*, *Mathematical Finance*, (To appear).
- [15] N. GANTERT, *Self-similarity of Brownian motion and a large deviation principle for random fields on a binary tree*, *Prob. Th. Rel. Fields*, 98 (1994), pp. 7–20.
- [16] J. GATHERAL, T. JAISSON, AND M. ROSENBAUM, *Volatility is rough*, *Quantitative Finance*, 18 (2018), pp. 933–949.
- [17] X. HAN AND A. SCHIED, *The hurst roughness exponent and its model-free estimation*, (2021).
- [18] C. M. HURVICH, E. MOULINES, AND P. SOULIER, *Estimating long memory in volatility*, *Econometrica*, 73 (2005), pp. 1283–1328.
- [19] J. JACOD AND P. PROTTER, *Discretization of processes*, vol. 67 of *Stochastic Modelling and Applied Probability*, Springer, Heidelberg, 2012.

- [20] A. LAHIRI AND R. SEN, *Fractional brownian markets with time-varying volatility and high-frequency data*, *Econometrics and Statistics*, 16 (2020), pp. 91–107.
- [21] J. LÉVY-VÉHEL, E. LUTTON, AND C. TRICOT, *Fractals in Engineering*, Springer, Berlin, 2005.
- [22] B. B. MANDELBROT AND J. W. VAN NESS, *Fractional Brownian motions, fractional noises and applications*, *SIAM Review*, 10 (1968), pp. 422–437.
- [23] Y. MISHURA AND A. SCHIED, *Constructing functions with prescribed pathwise quadratic variation*, *Journal of Mathematical Analysis and Applications*, 482 (2016), pp. 117–1337.
- [24] M. PODOLSKIJ AND M. VETTER, *Estimation of volatility functionals in the simultaneous presence of microstructure noise and jumps*, *Bernoulli*, 15 (2009), pp. 634 – 658.
- [25] L. ROGERS, *Things we think we know*, (2019). <https://www.skokholm.co.uk/wp-content/uploads/2019/11/TWTWKpaper.pdf>.
- [26] L. C. G. ROGERS, *Arbitrage with fractional Brownian motion*, *Mathematical Finance*, 7 (1997), pp. 95–105.
- [27] L. VIITASAARI, *Necessary and sufficient conditions for limit theorems for quadratic variations of gaussian sequences*, *Probab. Surveys*, 16 (2019), pp. 62–98.
- [28] W. WILLINGER, M. S. TAQQU, AND V. TEVEROVSKY, *Stock market prices and long-range dependence*, *Finance and stochastics*, 3 (1999), pp. 1–13.

Proof of Theorem 2.4 (i).

We will prove the result for $t = T$, for general t the proof generalizes without further complication. Since $q > p$ and the function x has finite p -variation along π , the pathwise q -th variation $[x]_{\pi}^{(q)}(t) = 0$ for all $t \in [0, T]$. Hence given any fixed $h > 0$ we have $[x]_{\pi}^{(q)}(t+h) - [x]_{\pi}^{(q)}(t) = 0$. Now given any $M > 0$ and any $n > 1$, we will show that $w(x, q, \pi)(t) > M$. For fix $n > 1$ we have:

$$\text{for all } t_i^n \in \pi^n, \quad [x]_{\pi}^{(q)}(t_{i+1}^n) - [x]_{\pi}^{(q)}(t_i^n) = 0.$$

Define the ‘unfeasible estimator’

$$w^n(x, q, \pi)(T) = \sum_{\pi^n} \frac{|x(t_{i+1}^n) - x(t_i^n)|^q}{[x]_{\pi}^{(q)}(t_{i+1}^n) - [x]_{\pi}^{(q)}(t_i^n)} \times (t_{i+1}^n - t_i^n).$$

Since $x \in V_{\pi}^p([0, T], \mathbb{R})$ for some $p > 0$, for fix large enough n , we have $\sum_{\pi^n} |x(t_{i+1}^n) - x(t_i^n)|^q \times (t_{i+1}^n - t_i^n) > 0$. So we get the lower bound of $w^n(x, q, \pi)$ as follows.

$$\begin{aligned} w^n(x, q, \pi)(T) &\geq \min_{t_i^n \in \pi^n} \left[\frac{1}{[x]_{\pi}^{(q)}(t_{i+1}^n) - [x]_{\pi}^{(q)}(t_i^n)} \right] \sum_{\pi^n} |x(t_{i+1}^n) - x(t_i^n)|^q \times (t_{i+1}^n - t_i^n) \\ &\geq C \left[\frac{1}{\max_{t_i^n \in \pi^n} ([x]_{\pi}^{(q)}(t_{i+1}^n) - [x]_{\pi}^{(q)}(t_i^n))} \right] = \infty > M. \end{aligned}$$

Since for all $n > 1$, $w^n(x, q, \pi)(t) = \infty$ we can conclude the following:

$$w(x, q, \pi)(t) = \lim_{n \rightarrow \infty} w^n(x, q, \pi)(t) = \infty.$$

Proof of Theorem 2.4(ii).

We will prove the result for $t = T$, for general t the proof follows exactly the same way. Since the function x has finite p -variation along π and $q < p$ from the assumption, the pathwise q -th variation $[x]_{\pi}^{(q)}(t) = \infty$ for all $t \in [0, T]$. Hence, given any fixed $h > 0$ we have $[x]_{\pi}^{(q)}(t+h) - [x]_{\pi}^{(q)}(t) = \infty$. Now given any $\epsilon > 0$ and any $n > 1$, we will show that $w(x, q, \pi)(t) < \epsilon$ by showing that $w^n(x, q, \pi)(t) < \epsilon$ for all large n . For fix $n > 1$ we have:

$$\begin{aligned}
& \text{for all } t_i^n \in \pi^n, \quad [x]_{\pi}^{(q)}(t_{i+1}^n) - [x]_{\pi}^{(q)}(t_i^n) = \infty. \text{ So,} \\
w^n(x, q, \pi)(T) &= \sum_{\pi^n} \frac{|x(t_{i+1}^n) - x(t_i^n)|^q}{[x]_{\pi}^{(q)}(t_{i+1}^n) - [x]_{\pi}^{(q)}(t_i^n)} \times (t_{i+1}^n - t_i^n) \\
&\leq \max_{t_i^n \in \pi^n} \left[\frac{|x(t_{i+1}^n) - x(t_i^n)|^q}{[x]_{\pi}^{(q)}(t_{i+1}^n) - [x]_{\pi}^{(q)}(t_i^n)} \right] \times \sum_{\pi^n} (t_{i+1}^n - t_i^n) \\
&\leq T \times \max_{t_i^n \in \pi^n} \left[\frac{|x(t_{i+1}^n) - x(t_i^n)|^q}{[x]_{\pi}^{(q)}(t_{i+1}^n) - [x]_{\pi}^{(q)}(t_i^n)} \right] \\
&\leq T \times \max_{t_i^n \in \pi^n} |x(t_{i+1}^n) - x(t_i^n)|^q \times \left[\frac{1}{\min_{t_i^n \in \pi^n} ([x]_{\pi}^{(q)}(t_{i+1}^n) - [x]_{\pi}^{(q)}(t_i^n))} \right] = 0 < \epsilon.
\end{aligned}$$

Since for all $n > 1$, $w^n(x, q, \pi)(t) = 0$;

$$w(x, q, \pi)(t) = \lim_{n \rightarrow \infty} w^n(x, q, \pi)(t) = 0.$$

Proof of Theorem 2.3

For convenience, assume $g(u) = \frac{d}{du} [x]_{\pi}^{(p)}(u)$. Since the p -th variation is strictly increasing we have $\sup_{t \in [0, T]} \frac{1}{g(u)} < \infty$. Since $g(u)$ is continuous in a compact interval $[0, T]$, it is also bounded. So for all $t \in [0, T]$, we have $\frac{1}{g(u)} \in (0, \infty)$. So as a consequence of mean value theorem,

$$\begin{aligned}
w^n(x, p, \pi)(t) &= \sum_{\pi^n \cap [0, t]} \frac{|x(t_{i+1}^n) - x(t_i^n)|^p}{[x]_{\pi}^{(p)}(t_{i+1}^n) - [x]_{\pi}^{(p)}(t_i^n)} \times (t_{i+1}^n - t_i^n) \\
&= \sum_{\pi^n \cap [0, t]} \frac{|x(t_{i+1}^n) - x(t_i^n)|^p}{g(u_i^n)},
\end{aligned}$$

where $u_i^n \in [t_i^n, t_{i+1}^n]$ for all $n \geq 1$ and for all $i = 0, \dots, N(\pi^n) - 1$. Finally, using properties of Riemann integral we can conclude:

$$\begin{aligned}
\sum_{\pi^n \cap [0, t]} \frac{|x(t_{i+1}^n) - x(t_i^n)|^p}{g(u_i^n)} &\xrightarrow{n \rightarrow \infty} \int_0^t \frac{1}{g(u)} d[x]_{\pi}^{(p)}(u) \\
&= \int_0^t \frac{d[x]_{\pi}^{(p)}(u)/du}{g(u)} du = \int_0^t du = t.
\end{aligned}$$

Since the limit always exists we can conclude the proof.

Proof of Example 2

Let B be a Wiener process on the canonical Wiener space $(\Omega, \mathcal{F}, \mathbb{P})$, i.e $\Omega = C^0([0, T], \mathbb{R})$, $B(t, \omega) = \omega(t)$ and \mathbb{P} is the Wiener measure. Let $\pi^n = (0 = t_0^n < t_1^n < \dots < t_{N(\pi^n)}^n = T)$ be a sequence of partitions of $[0, T]$ satisfying $|\pi^n| \log n \rightarrow 0$. Then the results of Dudley [13] imply that

$$\mathbb{P} \left(\sum_{\pi^n} |B(t_{i+1}^n \wedge t) - B(t_i^n \wedge t)|^2 \xrightarrow{n \rightarrow \infty} t \right) = 1.$$

So if we set $\Omega_0 = \Omega \cap Q_\pi([0, T], \mathbb{R})$ then $\mathbb{P}(\Omega_0) = 1$ and any $\omega \in \Omega_0$ satisfies $[\omega]_\pi(t) = t$. Now for any $\omega \in \Omega_0$ we also have the following:

$$\begin{aligned} w(\omega, 2, \pi)(t) &= \lim_{n \rightarrow \infty} w^n(\omega, 2, \pi)(t) = \lim_{n \rightarrow \infty} \sum_{\pi^n \cap [0, t]} \frac{(\omega(t_{i+1}^n) - \omega(t_i^n))^2}{[\omega]_\pi(t_{i+1}^n) - [\omega]_\pi(t_i^n)} \times (t_{i+1}^n - t_i^n). \\ &= \lim_{n \rightarrow \infty} \sum_{\pi^n \cap [0, t]} \frac{(\omega(t_{i+1}^n) - \omega(t_i^n))^2}{(t_{i+1}^n - t_i^n)} \times (t_{i+1}^n - t_i^n) = \lim_{n \rightarrow \infty} \sum_{\pi^n \cap [0, t]} (\omega(t_{i+1}^n) - \omega(t_i^n))^2 = t. \end{aligned}$$

So for Brownian motion, normalized quadratic variation is almost surely equal to t .

Remark 4. From Lemma 2 we know that, for any partition sequence π with $|\pi^n| \log(n) \rightarrow 0$, there exists $\Omega_\pi \subset \Omega$ with $\mathbb{P}(\Omega_\pi) = 1$ such that:

$$\forall \omega \in \Omega_\pi, \forall t \in [0, T], \quad w(\omega, 2, \pi)(t) = t.$$

We also have the following relation between quadratic variation and normalized-QV for Brownian paths in the class Ω_π .

$$\forall \omega \in \Omega_\pi, \forall t \in [0, T], \quad w(\omega, 2, \pi)(t) = [\omega]_\pi(t).$$

i.e. the null set for quadratic variation and normalized-quadratic variation of Brownian motion are the same.

Proof of Example 5

We give the proof for $p = 2$. For general p , the proof is provided in [10]. In [23] Schied has shown that for $x \in \mathcal{X}^2$, the quadratic variation along the dyadic partition is linear: $[x]_{\mathbb{T}}(t) = t$. So:

$$\begin{aligned} w^n(x, p = 2, \mathbb{T})(t) &= \sum_{\mathbb{T}^n \cap [0, t]} \frac{(x(\frac{i+1}{2^n}) - x(\frac{i}{2^n}))^2}{[x]_{\mathbb{T}}(\frac{i+1}{2^n}) - [x]_{\mathbb{T}}(\frac{i}{2^n})} \times \left(\frac{i+1}{2^n} - \frac{i}{2^n} \right) \\ &= \sum_{\mathbb{T}^n \cap [0, t]} \left(x\left(\frac{i+1}{2^n}\right) - x\left(\frac{i}{2^n}\right) \right)^2 \xrightarrow{n \rightarrow \infty} t. \end{aligned}$$

This concludes the proof.